Experimental and Computational Study of the Group 1 Metal Cation Chelates with Lysine: Bond Dissociation Energies, Structures, and Structural Trends

Amy A. Clark,[†] Bo Yang,[‡] M. T. Rodgers, [‡] and P. B. Armentrout*[†]

[†]Department of Chemistry, University of Utah, 315 South 1400 East, Room 2020, Salt Lake City, Utah 84112, United States

[‡]Department of Chemistry, Wayne State University, Detroit, Michigan 48202, United States

Abstract: The kinetic energy dependence of the collision-induced dissociation (CID) of Group 1 metal cations (M^+ = Li^+, Na^+, K^+, Rb^+, and Cs^+) chelated to the amino acid lysine (Lys) were measured by threshold CID (TCID) using a guided ion beam tandem mass spectrometer. The simple loss of neutral lysine is the only dissociation channel observed with the heavier alkali metal cations, whereas CID of Li^+(Lys) yields other competing channels including loss of NH_3 (the dominant channel at low energy) and eight other reactions. Analysis of the kinetic energy dependent cross sections yields experimental M^+(Lys) bond dissociation energies (BDEs) of 376 ± 30, 219 ± 13, 160 ± 10, 141 ± 6, and 128 ± 4 kJ/mol for Li^+, Na^+, K^+, Rb^+, and Cs^+, respectively. Computational searches yielded eighteen distinct, low-energy structural families related to sites of M^+ binding in M^+(Lys) complexes, and ten distinct, low-energy structural families for neutral lysine. Among the four levels of theory and three basis sets used, four different ground conformers of M^+(Lys) and four different ground conformers of lysine were found, including a ground conformer of K^+(Lys) and Cs^+(Lys), [N_ε,CO(OH)] and its higher energy zwitterionic analogue, [N_ε,CO_2^-], that better explains recent infrared multiple photon dissociation (IRMPD) action spectroscopy results. Computational results for predicted ground structures of M^+(Lys) complexes yielded computed BDEs in reasonable agreement with experiment.

1. INTRODUCTION

Many proteins and peptides have Group 1 metal ions coordinated via electrostatic interactions to one or more of the side chains and/or the secondary amines and carbonyl oxygens on the backbone. It is worthwhile to determine the primary bond dissociation energies (BDEs) between individual amino acid residues and alkali ions in the gas phase as an initial reference to those found physiologically in proteins and peptides. With a single terminal amine on its side chain, the basic amino acid lysine (Lys) offers a simple, flexible ligand for these Group 1 cations. Compared to peptides, many of the M^+(Lys) binding motifs for the free amino acid are unique because the hydroxyl oxygen (which cannot be present except at the C-terminus in a peptide) can actively chelate the metal cation. However, physiologically, similar binding motifs are plausible in peptides except a water molecule solvates the metal cation in lieu of the hydroxyl moiety.

The physiology of the Group 1 metal cations is broad. Na^+ and K^+ are ubiquitous.[1] Li^+ is not but may be a beneficial trace mineral[2-3] and is widely administrated therapeutically to patients with bipolar affective disorder[4-5] because of its efficacy. With therapy and because Li^+ has a low clearance rate,[6] it becomes pervasive in tissues of these patients over time.[7] It accumulates in plasma and is actively extruded from red blood cells.[8-9] It also accumulates in muscle tissue and other organs, and more slowly into brain tissue.[7] Li^+ targets white matter versus grey matter in brain tissue of depressive patients, but not in normal control subjects treated with lithium.[10-11] Li^+ transport across cell membranes uses the Na channel and Na/H exchanger and other tissue-specific Na^+ transport channels.[12]

With respect to the heavier Group 1 metal cations, the $^{82}Rb^+$ isotope is used to image tissues and tumors[13-14] and to study disruption to the blood-brain barrier (BBB).[14] Such studies are possible because of the ability of Rb^+ and Cs^+ to bind in K^+ channels,[15] with clearance rates at or below that of K^+.[16] Radioactive $^{134}Cs^+$ and $^{137}Cs^+$ have also recently evolved as environmental toxins, a result of atmospheric nuclear weapons tests in the mid-19th century and following the 1986 Chernobyl[17] and 2011 Fukushima[18] accidents. Cs^+ readily chelates to many organic

molecules,[19] including humic and fulvic acids, which are common organic acids in soil,[20] and has severe cardio pathophysiological consequences in humans exposed to those environments.[21]

All five of the Group 1 metal cations Li^+ through Cs^+ are presented here to highlight binding trends to lysine. In previous work, Group 1 metal binding trends to amino acids (AA) follow the trend $Li^+(AA) > Na^+(AA) > K^+(AA) > Rb^+(AA) > Cs^+(AA)$, a consequence of the increasing size of the metal cations as they get heavier.[22-23] This has been shown for Asn, Asp, Glu, and Gln;[24-26] Cys;[27-29] Gly;[29-32] His;[33-34] Met;[35-36] Phe;[34,36-37] Pro;[29,32,38] Ser;[29,32,39] Thr;[29,32,39] Trp;[34,36-37] and Tyr.[34,36-37] Infrared multiphoton dissociation spectroscopy (IRMPD) together with theory has in many cases elucidated the structures of the ground conformers of $M^+(AA)$ (M^+ = Li^+, Na^+, K^+, Rb^+ and Cs^+) for $M^+(Arg)$,[40-41] $M^+(Asn)$,[42] $M^+(Asp)$,[43] $M^+(Cys)$,[44] $M^+(Gln)$,[45] $M^+(Glu)$,[43] $M^+(Gly)$,[46] $M^+(His)$,[47] $M^+(Lys)$,[48-49] $M^+(Met)$,[50] $M^+(Phe)$,[51-52] $M^+(Pro)$,[46,53-54] $M^+(Ser)$,[55] $M^+(Thr)$,[56] $M^+(Trp)$,[57] and $M^+(Tyr)$.[51] (Here we use the term ground conformer to denote the lowest energy structure, avoiding the use of "state" as all conformers considered lie on the same electronic singlet state surface.) These studies show that the identity of the ground conformer depends on the size of the metal cation. Interestingly, identification of the ground structure of $K^+(Lys)$ appears incomplete,[48] and hence is revisited here.

In most cases, low-energy collision-induced dissociation (CID) of $M^+(AA)$ (M^+ = Na^+, K^+, Rb^+, and Cs^+) results in the simple loss of the intact neutral AA ligand. Some $Na^+(AA)$[24,34,58] and many $Li^+(AA)$[27,34,59-60] exhibit more complex fragmentations. Such findings parallel those in the present study, where CID of $M^+(Lys)$ (M^+= Na^+, K^+, Rb^+, and Cs^+) results in the simple loss of neutral lysine, whereas $Li^+(Lys)$ has nine dissociation channels competing with loss of neutral lysine. These competing channels are dominated by the primary loss of the side chain amine, $N_\varepsilon H_3$.[61-62] Modeling of these CID cross sections provides M^+-Lys bond dissociation energies (BDEs), which compare favorably with computational values obtained at several levels of theory. The latter require a thorough theoretical investigation of the structures of the $M^+(Lys)$ complexes, which also provides molecular parameters needed for the modeling.

2. EXPERIMENTAL AND COMPUTATIONAL SECTION

2.1. Mass Spectrometry

All data were collected using an electrospray ionization (ESI) source[63] and either the Utah or Wayne State guided ion beam tandem mass spectrometers (GIBMS), previously described in detail[64-66] and briefly below. Stock solutions of lysine and M^+ ($M^+ = Na^+$, K^+) were combined to achieve approximately 10^{-4} M of both lysine and M^+ in 50:50 (v/v) methanol/water. Solutions of $M^+ = Li^+$, Rb^+, Cs^+ gave the best intensities of M^+(Lys) using higher (~ 10^{-3} M) M^+ concentrations in 100% methanol ($M^+ = Li^+$) and 1 – 5 × 10^{-4} M in 50:50 (v/v) methanol/water ($M^+ = Rb^+$ and Cs^+). Ions were introduced into the source region through a heated (110 – 120 °C) capillary (the ion source anode). They were then collected by a radiofrequency (rf) ion funnel[67] that focuses into a rf-only hexapole ion guide, where the ions are thermalized by ~10^4 collisions with ambient gas.[24,63,68-70] The ions were extracted from the source and focused into a magnetic momentum analyzer to select the desired M^+(Lys) reactant ion, after which the beam was focused and decelerated to a well-defined kinetic energy (the nominal laboratory energy) before entering a rf-only octopole ion guide,[64-65,71] which confines the ions in the radial direction.

Once in the octopole, ions drifted through the reaction cell, which contained the reactant neutral xenon. Xe was used as the collision gas because it is atomic, neutral, relatively large and polarizable, such that the kinetic to internal energy deposition upon collision is relatively high.[72-73] Data were collected at several Xe pressures (~0.2, 0.1, and 0.05 mTorr), such that extrapolations to zero pressure ensure that only single-collision conditions apply.[64,74] Following collision-induced dissociation (CID), reactant and product ions drifted to the final focusing stage, where they were extracted, focused into a quadrupole mass filter for mass analysis, and counted with a Daly detector.[75] Absolute reaction cross sections were generated from the ion intensities after correcting for background signals as described previously.[64] Absolute uncertainties in the cross section magnitudes are ±20% with relative uncertainties of ±5%. Collision energies were converted from the laboratory (lab) frame to the center-of-mass (CM) frame using $E_{CM} = E_{lab} \times M/(m + M)$, where M is the mass of the neutral reactant (Xe) and m is the mass of the M^+(Lys)

reactant ion. In the discussion below, all energies are in the CM frame unless otherwise noted. The absolute zero and distribution of the ion kinetic energies was determined using a retarding technique, as previously outlined.[64]

2.2. Threshold analysis

All of the fragmentation reactions observed in this work are endothermic. Threshold energies at 0 K for these processes (E_0) can be obtained by modeling the data using the semi-empirical eq 1.

$$\sigma(E) = \sigma_0 \sum_i \frac{g_i (E + E_i - E_0)^n}{E} \quad (1)$$

This equation relates the energy-dependent CID cross-section, $\sigma(E)$, to the energy-independent and adjustable parameter σ_0; the energies (E_i) and populations (g_i) of the rovibrational states i of the reactant ion where $\sum g_i = 1$; the relative kinetic energy E of the reactants in the CM frame; and the adjustable parameter n, which describes the efficiency of energy deposition during collision.[65] A Maxwell-Boltzmann distribution at 300 K describes the relative populations, g_i. The vibrational frequencies and rotational constants used to calculate E_i and g_i are obtained from quantum mechanical calculations described in the next section.

In order to compare the model of eq 1 to the data, two other considerations must be made. First, the distributions of the kinetic energies of the reactant ion and neutral (Doppler broadening)[76] were accounted for by explicitly convoluting eq 1 over both reactant kinetic energy distributions.[64] Second, the lifetime of the fragmenting complexes may exceed the experimental time available for dissociation (τ = ~5 × 10^{-4} s in the Utah GIBMS and ~1 × 10^{-4} s in the Wayne State GIBMS),[65-66] leading to a kinetic shift, i.e., a higher apparent threshold. This shift can be estimated by incorporating statistical Rice-Ramsperger-Kassel-Marcus (RRKM) theory[77-79] into eq 1,[80-81] yielding eq 2, which includes the integration over the unimolecular dissociation probability and the possibility of competitive channels,[81] which is needed to analyze the data for Li^+(Lys).

$$\sigma_j(E) = \frac{n\,\sigma_{0,j}}{E} \sum g_i \int_{E_{0,j}-E_i}^{E} \frac{k_j(E^*)}{k_{tot}(E^*)} \left\{1 - e^{-k_{tot}(E^*)\tau}\right\} (E - \epsilon)^{n-1} d(\epsilon) \quad (2)$$

Here, $\sigma_{0,j}$ is the energy-independent adjustable scaling parameter for channel j; $E_{0,j}$ represents the threshold energy for channel j at 0 K; ϵ is the energy transferred from translation into the internal energy of the complex during the collision; the internal energy of the energized molecule (EM) after the collision is $E^* = \epsilon + E_i$; and n, g_i, E_i, τ, and E are defined as above. The unimolecular rate constant $k_j(E^*)$ for dissociation channel j of the EM is defined by RRKM theory in eq 3,

$$k_{tot}(E) = \sum_j k_j(E^*) = \sum_j s_j N^{\dagger}_{j,vr}\left(E^* - E_{0,j}\right)/h\rho_{vr}(E^*) \qquad (3)$$

where $N^{\dagger}_{j,vr}(E^* - E_{0,j})$ is the sum of the rovibrational states of the transition state (TS) for channel j at an energy $E^* - E_{0,j}$; $\rho_{vr}(E^*)$ is the density of rovibrational states of the EM at the available energy E^*; s_j is the reaction degeneracy for channel j ($s_j = 1$ in all cases here), and h is Planck's constant. The density and sum of the rovibrational states were determined with the Beyer-Swinehart-Stein-Rabinovitch algorithm.[82-83] When $k_{tot}(E^*)$ is faster than the time available, the integration in eq 2 recovers eq 1. Most of the CID reactions are limited by loose TSs, so that most TS frequencies equal those of the dissociated products and the transitional frequencies were treated as rotors in the phase space limit (PSL), as discussed in detail elsewhere.[80-81] The 2D external rotations were treated adiabatically but with centrifugal effects included[83] and the rotational energy was treated using a statistical distribution summed over all possible values of the rotational quantum number. For the loss of ammonia from Li^+(Lys), the reaction is limited by a tight TS, for which molecular parameters were taken directly from theoretical results for the rate-limiting TS structure.

2.3. Computational Details

To obtain the frequencies used in modeling the experimental data and to provide insight into trends in the metal ion binding, the gas-phase ground and low-lying conformers of neutral Lys and M^+(Lys) need to be identified. In order to achieve this, an array of low-lying, computational structures was examined using molecular mechanics and Hartree-Fock methods (HF/3-21G). Initial structures of neutral lysine, Li^+(Lys), Na^+(Lys), and K^+(Lys) were submitted for simulated annealing using the AMBER program and the AMBER force field.[84] This process

was repeated 6 - 18 times or until new structures failed to appear at relative energies less than about 60 kJ/mol. The annealing process did not yield all structural families in all M^+(Lys), but comparable structures were created as necessary by substitution of all metal ions. In particular, charge-solvated and zwitterionic forms of related structures were explored when relevant. Neutral lysine structures were also compared with results from recent matrix-isolation FT-IR spectra and theory of gaseous lysine.[85-86] Structures between 0 – 60 kJ/mol that exhibited similar energies were manually compared to identify unique structures for higher level geometry optimizations. These calculations were performed using the Gaussian09 suite of programs[87] at the B3LYP level of theory using the 6-311+G(d,p) basis set including frequency calculations. Using these geometries, single point energies (SPEs) were calculated using B3LYP, B3P86, and MP2(full) levels of theory with the 6-311+G(2d,2p) basis set. For simplicity below, these SPEs will be referred to only as B3LYP, B3P86, and MP2 without re-specifying the basis set or geometry optimization step.

For Li^+(Lys), the resulting B3LYP/6-311+G(d,p) geometries were also geometry optimized using the MP2(full) level of theory and the cc-pVDZ(Li-C) basis set, where (Li-C) denotes additional core polarization functions on lithium (cc-pCVDZ).[88] Single point energies were then calculated using B3LYP, B3P86, and MP2(full) levels of theory with the basis set aug-cc-pVTZ(Li-C). It has been demonstrated elsewhere that including the core electrons on lithium as well as ignoring counterpoise corrections is required for adequate reproduction of thermodynamic information regarding Li^+ complexes.[31] The notations B3LYP/pCVTZ, B3P86/pCVTZ, and MP2/pCVTZ will be used to refer to these SPEs below, or pVTZ when not referring to Li^+ complexes.

Low-lying conformers of K^+(Lys) were used as starting points for Rb^+(Lys) and Cs^+(Lys) structures. For M^+(Lys) (M^+ = K^+, Rb^+, and Cs^+), geometries were further optimized and frequencies determined using the B3LYP level of theory with the def2-TZVPPD basis set.[29,32,89] Single point energies were calculated using B3LYP, M06, and MP2(full) levels of theory with the same basis set. M06 was chosen because of its successful applications in organometallic and

noncovalently bound systems.[90] The notations B3LYP/def2, M06/def2, and MP2/def2 will be used to refer to these calculations below.

Additionally, transition state (TS) structures for loss of $N_\varepsilon H_3$ from Li^+(Lys) were explored starting from several low-energy conformers of Li^+(Lys). Intrinsic reaction coordinate (IRC) calculations were used to connect the TS structures with the minima on either side. The lowest energy TS located yields the best reproduction of the data and hence is used exclusively in the present work. SPEs of this structure were obtained using B3LYP, B3P86, and MP2 levels of theory with the 6-311+G(2d,2p) and aug-cc-pVTZ(Li-C) basis sets. The complete details of the CID of Li^+(Lys) + Xe will be the subject of a future publication.

For all Lys and M^+(Lys) conformers, zero-point vibrational energy (ZPE) corrections were obtained at the B3LYP/6-311+G(d,p), MP2(full)/cc-pVDZ(Li-C), or B3LYP/def2-TZVPPD levels after scaling by 0.989.[91] Basis set superposition errors (BSSE) in the computed BDEs for M^+(Lys) complexes were estimated using the full counterpoise (cp) method.[92]

3. RESULTS

3.1. Theoretical Results: Structures of Lysine

The computational procedure described above yielded ten distinct, low-lying (< 30 kJ/mol) structural families for neutral lysine (see Figures 1 and S1), all of which are charge-solvated (CS) or non-zwitterionic. As with other researchers,[85-86] we found no low-lying, stable zwitterionic (ZW) lysine structures in the gas phase. Here, the distinct families of low-lying structures for neutral lysine are described by their internal hydrogen bonds followed by a designation of major dihedral angles that distinguish members within the same family. For instance, [OH-O-H_2N_α]tgtttt$_+$ (Figure 1a) has intramolecular hydrogen bonds between the hydroxyl group hydrogen (OH) and carbonyl oxygen (O), and bifurcated hydrogen bonding between the backbone amino group ($N_\alpha H_2$) and carbonyl oxygen (O). Neutral lysine and M^+(Lys) structures have six major dihedral angles, beginning with the hydrogen on the hydroxyl oxygen (or the hydrogen nearest the hydroxyl oxygen in a zwitterionic structure) to the α-carbon,

$\angle HOCC_\alpha$, $\angle OCC_\alpha C_\beta$, and so forth continuing along the carbon atoms of the side chain and ending at N_ε with $\angle C_\gamma C_\delta C_\varepsilon N_\varepsilon$ (see Figure 1a for labels). The angles are designated as c (cis, for angles of 0 - 45°), g (gauche, 45 - 135°), and t (trans, 135 - 180°). In some cases, the sign of the dihedral angle (+/–) is needed to differentiate structures. All three approaches used for geometry optimization (B3LYP/6-311+G(d,p), MP2(full)/cc-pVDZ, and B3LYP/def2-TZVPPD) generally yielded the same dihedral angle designations and signs for a particular structure; however, minor changes from B3LYP/6-311+G(d,p) optimized structures are detailed in Table S1.

Of the neutral lysine structures located, four are the ground conformer at different levels of theory and basis set (Figure 1a – 1d), with relative energies listed in Table 1. [OH-O-H_2N_α]tgtttt$_+$ (Figure 1a) is the ground conformer at B3LYP and B3LYP/def2 levels of theory, in agreement with the B3LYP results of Boeckx and Maes (which they called LYS14).[85] We find the very similar [OH-O-H_2N_α]tgtttt$_-$ structure (Figure 1b) is the ground conformer at B3LYP/pVTZ. These two structures differ only in the orientation of the $N_\varepsilon H_2$ side-chain group. Both are entropically favorable structures because the side chain is free from hydrogen bonding, which allows for considerable flexibility. [OH-N_ε,CO-H_2N_α]cggggg$_-$ (Figure 1c) is the ground structure at MP2 levels of theory with all basis sets (again in agreement with the MP2 ground structure found by Boeckx and Maes, LYS1, and the B3LYP and MP2 ground structure found by Leng et al.[86]), as well as for the B3P86 and M06/def2 levels. It is the most compact ground conformer because of its extensive hydrogen bonding. [OH-N_ε,CO-H_2N_α]cgtggg (Figure 1e) is another structure in the same family and is within 2 kJ/mol of the ground structure at the B3P86, M06, and MP2 levels of theory. [OH-N_αH-N_ε]cgttgg$_-$ (Figure 1d) is the B3P86/pVTZ ground structure. This and other conformers, all of which are included in the Supporting Information, Figure S1 and Table S1, have intermediate levels of hydrogen bonding across the lysine molecule. The Supporting Information also describes a comparison with the literature results in more detail.

3.2. Theoretical Results: Structures of Metallated Lysine

Our search for conformers of M^+(Lys) located eighteen distinct, low-lying (< 30 kJ/mol) structural families (see Figure S2). Four of these were the ground conformer at some level of theory and basis set and are shown in Figure 2 for K^+(Lys). Table 2 lists the relative energies of the four possible ground conformers with M^+ = Li^+, Na^+, K^+, Rb^+, Cs^+. Table S2 lists such information for all conformers located and Table S3 provides characteristic structural parameters for all conformers. The structures are distinguished by chemical symbols in square brackets indicating the oxygen and nitrogen atoms chelated to M^+, followed by a designation of the six dihedral angles to distinguish members within the same family. For zwitterionic [CO_2^-] and the related [COOH] structures, superscripts α and β follow the convention established by Bush et al.,[48] with an additional designation α2 located in the present work. An α designates that $N_\varepsilon H_3^+$ donates hydrogen bonds (H-bonds) to N_α and CO; whereas in α2, $N_\varepsilon H_3^+$ donates a H-bond only to CO because the N_α is trans to the hydroxyl oxygen. For the [COOH]$^\alpha$ analogues, the CO•••HN$_\varepsilon$ H-bond in [CO_2^-]$^\alpha$ conformers is replaced by COH•••N$_\varepsilon$. A β indicates that $N_\alpha H_3^+$ donates a H-bond to N_ε and CO. For the [COOH]$^\beta$ analogues, the CO•••HN$_\alpha$ H-bond in [CO_2^-]$^\beta$ conformers is replaced by COH•••N$_\alpha$.

In agreement with previous work,[48,93] the ground conformers of Li^+(Lys) and Na^+(Lys) across all levels of theory and basis sets are charge-solvated tridentate structures, [N$_\alpha$,N$_\varepsilon$,CO]t$_+$gggtg (Figure 2a and Table 2). IRMPD spectroscopy strongly supports these theoretical findings.[48] In contrast, the ground conformers of K^+(Lys), Rb^+(Lys), and Cs^+(Lys) depend on theory and basis set. The zwitterionic and bidentate [CO_2^-]$^\beta$cgtgg$_+$g (Figure 2c) is the ground conformer for all three metals using B3LYP with any basis set and using B3P86 for K^+(Lys). The similar conformer [CO_2^-]$^\beta$cggggg (Figure 2e) is the ground conformer of K^+(Lys) using MP2. At the M06/def2 and MP2/def2 levels, the present study indicates that K^+(Lys), Rb^+(Lys), and Cs^+(Lys) ground structures are charge-solvated, tridentate [N$_\varepsilon$,CO(OH)]cggggt (Figure 2b and Table 2). As described more completely in the Supporting Information, the [N$_\varepsilon$,CO(OH)] designation indicates that the chelation from the hydroxyl moiety is midway between tridentate [N$_\varepsilon$,COOH] and bidentate [N$_\varepsilon$,CO]. This effect is quantified in the Supporting

Information by evaluating the ratio of the four metal-ligand bond distances [M^+-OC : M^+-OH : M^+-N_α : M^+-N_ε], which naturally accounts for the variation in bond distances associated with metal cation size. The Supporting Information also compares the present results for the structures of K^+(Lys) and Cs^+(Lys) with those from Williams and coworkers.[48-49] Reasonable agreement is found in both studies although we located some structures not previously considered, as detailed in the next section.

3.3. Theoretical Results: Comparison to IRMPD

In their previous work, Williams and coworkers suggested that both K^+(Lys) and Cs^+(Lys) were dominated by non-zwitterionic structures along with substantial contributions from zwitterionic species.[48-49] No definitive assignments of particular structures were made in part because their calculations indicated the ground structure for K^+(Lys) was zwitterionic, OO^{β}-ZW (our [CO_2^-]$^{\beta}$cggggg), with N_{SC}O-NZ and N_{SC}OO-NZ (our [N_ε,CO]cggg$_+$t$_+$g$_+$ and [N_ε,CO(OH)]cggggt, respectively) being competitive for Cs^+(Lys) at the MP2 level. In contrast, the present study indicates that the ground conformer is [N_ε,CO(OH)]cggggt for K^+(Lys), Rb^+(Lys), and Cs^+(Lys). As this ground conformer may better explain the IRMPD results, we reexamine the K^+(Lys) and Cs^+(Lys) spectra in light of this new information because it is helpful to establish the M^+(Lys) ground conformers in order to most accurately model the TCID data.

Figure 3 shows the published IRMPD spectra from Williams and coworkers[48-49] compared with our calculated spectra for K^+(Lys) and Cs^+(Lys) from B3LYP/def2 optimized structures. K^+(Lys) spectra optimized using B3LYP are similar and are shown in the Supporting Information. Experimentally, the two spectra are similar with intense bands at ~1740 and ~1400 cm^{-1} and a prominent band at ~1600 cm^{-1}.[48-49] These bands can usually be associated with the carbonyl stretch, COH bend with H-bonding to N_α, and the NH_2 scissors bends of both amino groups, respectively, of a charge solvated species. Both spectra also exhibit bands near 1460 and 1670 cm^{-1}, which can be identified as the bonded CNH bend of a protonated amine group and the carbonyl stretch, respectively, in a [CO_2^-] zwitterionic species.[48,57] These latter bands are somewhat larger for Cs^+(Lys) than for K^+(Lys), indicating a relatively larger contribution from a

zwitterion.

For both K^+(Lys) and Cs^+(Lys), [N_ε,CO(OH)]cggggt is the lowest Gibbs energy structure at 298 K using M06/def2 and MP2/def2 levels of theory, Table 3. Each of these structures nicely reproduces the bands at 1400, 1600, and 1740 cm^{-1}, particularly the latter band, Figure 3. (The bands at ~1600 cm^{-1} are red-shifted compared to theory, which is typical in IRMPD spectra of M^+(AA) systems because of the appreciable anharmonicity in the NH_2 bend.[94-97]) There are other CS structures in Figures S3 and S4, notably [N_ε,CO]cggg$_+$t$_+$g$_+$, that exhibit bands that match the experimental spectra, but they are all calculated to lie ≥ 4 kJ/mol higher in relative Gibbs energy, Table 3. The zwitterionic contributions to the spectra at 1460 and 1670 cm^{-1} could derive from [CO_2^-]$^\beta$cggggg or [CO_2^-]$^\beta$cgtgg$_+$g, which both have low relative Gibbs energies at some levels of theory, but the best spectral match for both K^+(Lys) and Cs^+(Lys) is [N_ε,CO_2^-]cggggt, which has a band at ~1670 cm^{-1}. (This observation was also made by Williams and coworkers.[49]) Although its relative Gibbs energies (all ≥ 17 kJ/mol, Table 3) apparently do not support its contribution, it can be realized that this structure is directly related to the [N_ε,CO(OH)]cggggt structure by motion of the proton between O and N_α, compare Figure 2b and 2d. As a consequence, these two structures occupy the same asymmetric double-well potential, such that the zero-point motion of this proton directly couples the two structures. This situation is shown in more detail in Figure S6 for K^+, Rb^+, and Cs^+. This diagram shows that the zero-point energy of the harmonic proton motion associated with this potential in the [N_ε,CO(OH)] structure (the OH•••N_α stretch, ~19.2 kJ/mol for all three metals) is comparable to the barrier height between the [N_ε,CO(OH)] and [N_ε,CO_2^-] forms for all three metal cations. More importantly, the barrier is significantly *below* the zero-point energy of this motion (the N_αH•••O stretch, ~15.7 kJ/mol for all three metals) in the zwitterionic form. Although the actual energy of this vibration is certainly strongly affected by the anharmonicity of the asymmetric double-well potential, it should still be the case that the ground state vibrational wavefunction associated with this proton motion quantum mechanically has amplitude in both coupled potential wells associated with the non-zwitterionic and the zwitterionic species. A similar result has also been observed previously

for Cs^+(Ser).[55] Thus, the IRMPD spectrum for both K^+(Lys) and Cs^+(Lys) can be assigned to the [N_ε,CO(OH)]cggggt structure, which is quantum mechanically directly coupled with the [N_ε,CO_2^-]cggggt structure. Thus, IR absorption in the *orthogonal* vibrational modes probed in the IRMPD experiments is sensitive to both structures. As can be seen in Figure 3, superpositions of the harmonic contributions from both structures provide very good reproductions of the experimental spectra for both complexes.

Altogether, our theoretical results compared with the experimental spectra suggest that both K^+(Lys) and Cs^+(Lys), and presumably Rb^+(Lys), are predominantly [N_ε,CO(OH)] along with a contribution from the zwitterionic [N_ε,CO_2^-]. On the basis of the spectroscopy, contributions from other conformers cannot be ruled out but are not needed to explain the observed spectra and are unlikely given the calculated relative Gibbs energies. This conclusion agrees with the more general observations of Williams and coworkers, although the coupling between the two structures was not previously identified and the [N_ε,CO(OH)] species were not identified theoretically as the ground structures.

3.4. Cross Sections for Collision-Induced Dissociation and Data Analysis.

Figure 4 shows representative zero-pressure extrapolated data sets for CID of the alkali metal cation complexes with lysine. A cursory examination of the data shows the expected trend in the BDEs: D(Li^+-Lys) > D(Na^+-Lys) > D(K^+-Lys) > D(Rb^+-Lys) > D(Cs^+-Lys). The only dissociation pathway observed for Na^+(Lys), K^+(Lys), Rb^+(Lys), and Cs^+(Lys) is the loss of intact lysine, reaction 4.

$$M^+(Lys) + Xe \rightarrow M^+ + Lys + Xe \qquad (4)$$

The model of eq 2 was used to analyze the threshold regions of the Na^+(Lys), K^+(Lys), Rb^+(Lys), and Cs^+(Lys) data and reproduces these well over energy ranges of 5, 4, 2, and 2 eV, respectively, as also shown in Figure 4. The threshold energy, E_0, obtained is a direct measure of the bond dissociation energy (BDE) of M^+-Lys at 0 K. A detailed discussion of the various approaches to modeling the data can be found in the Supporting Information. The recommended

optimized fitting parameters for eq 2 are provided in Table 4.

As discussed in the Supporting Information, data were interpreted allowing the M^+(Lys) complex to dissociate to either the compact neutral conformer of Lys ([OH-N_ε,CO-H_2N_α]cggggg–, the B3P86 and MP2 ground structure) or the extended neutral conformer ([OH-O-H_2N_α]tgtttt+, the B3LYP ground structure) or both. In all cases, it is clear that dissociation to the extended conformer is strongly favored entropically (see Figure S7) such that modeling results assuming dissociation to the extended conformer are believed to lead to our best experimental values. This choice is independently validated by comparison with theoretical values, as detailed in the next section,

For Na^+(Lys), which clearly has a [N_α,N_ε,CO]t+gggtg ground structure, our best model leads to a threshold of 2.27 ± 0.14 eV, Table 4. For M^+(Lys) where $M^+ = K^+$, Rb^+, and Cs^+, there are several different possible ground conformers of each reactant. For K^+(Lys), Rb^+(Lys) and Cs^+(Lys), models including [N_εCO(OH)]cggggt (as identified in the IRMPD spectrum), [N_ε,CO_2^-]cggggt (which also contributes to the IRMPD spectrum), and [CO_2^-]$^\beta$cgtgg+g (the B3LYP, B3P86, and B3LYP/def2 ground structure) were all considered, Table 4. We utilize a weighted average of all three of these threshold values as our best determination, and include an uncertainty that is two weighted standard deviations. This approach leads to final values of 1.66 ± 0.10, 1.46 ± 0.06, and 1.32 ± 0.04 eV for K^+(Lys), Rb^+(Lys), and Cs^+(Lys), respectively.

Analysis of the Li^+(Lys) results is more complicated because of the additional reaction channels that start at energies below that for the Li^+ channel of reaction 4, Figure 4a. For Li^+(Lys) decomposition, there are nine channels competing with the loss of neutral lysine. Pathways for the other competing reactions have been explored computationally elsewhere[98] and are beyond the scope of the present publication. The primary loss of NH_3 dominates the competing channels. This product is formed by the loss of the side chain amine, as was demonstrated with $^{15}N_\varepsilon$-labeled protonated lysine,[62] and outlined theoretically.[98] This leads to a product that is a derivative of norleucine, lithiated 2-amino-5-hexenoic acid, which we refer to as Li^+(Nle). To accurately analyze the threshold for reaction 4 with Li^+(Lys), the effect of

competition with these other channels must be included, as discussed in the Supporting Information. Figure 4a shows the competitive fit for the Li^+(Lys) system, which reproduces the data over a range in energy up to about 9 eV. This model uses the tridentate reactant [N_α,N_ε,CO]t_+gggtg and the extended [OH-O-H_2N_α]tgtttt$_+$ conformer of lysine, and yields thresholds of 1.40 ± 0.09 and 3.93 ± 0.11 eV for loss of $N_\varepsilon H_3$ and Lys, respectively, Table 4. A threshold for reaction 4 of 3.86 ± 0.12 eV is obtained if molecular parameters obtained using the cc-pVDZ basis set are used instead. Here, we adopt the average threshold value of 3.90 ± 0.30 eV (two standard deviations) as our best threshold determination for reaction 4 with Li^+(Lys).

Thresholds were also determined using eq 1 in which the kinetics of dissociation are ignored. This permits determination of the kinetic shifts, which range from ~3 eV for Li^+(Lys) to ~0.8 eV for Na^+(Lys) and down to about 0.3 eV for Cs^+(Lys). The very large shift for Li^+(Lys) is partly attributable to the competition with the other lower energy dissociation channels and partly to the much higher threshold energy. On average, the $\Delta S^\dagger_{1000}$ values for the loose PSL TS leading to M^+ + Lys are 60 - 90 J/K mol when the extended lysine conformer is used and 10 - 40 J/K mol with the compact conformer, again illustrating that the former is entropically favored.

4. DISCUSSION

Our final experimental BDEs for the eight complexes investigated here are provided in Table 5. We also convert these 0 K BDEs to 298 K bond enthalpies and 298 K Gibbs energies of dissociation, as listed in Table S6 of the Supporting Information. Because these conversions depend on the specific conformers involved, multiple values are provided.

4.1. Comparison of literature, experimental, and theoretical thermochemistry

The only available literature value among the alkali metal cations bound to lysine comes from kinetic method studies of Wesdemiotis and coworkers.[99-100] For Na^+(Lys), they determined a lower limit of >213 ± 8 kJ/mol, in good agreement with the absolute value determined here of 219 ± 13 kJ/mol.

The experimental M^+-Lys BDEs are compared with theory in Table 5 and plotted in Figure 5. In previous work on a series of lithium cation complexes with a variety of ligands,[31] it was shown that including polarization of the 1s core electrons as well as advanced levels of theory were needed to replicate experiment. It was suggested that the MP2/pCVTZ level of theory *excluding* counterpoise corrections provided reasonable results at a reasonable computational cost. This level of theory predicts a Li^+(Lys) BDE of 321 kJ/mol, and B3LYP, B3LYP/pCVTZ, and B3P86/pCVTZ provide similar values (320 – 329 kJ/mol). These values agree within experimental uncertainty with the experimental value obtained using the compact neutral, 331 ± 26 kJ/mol, but are well below that obtained assuming the extended neutral, 376 ± 30 kJ/mol. In both cases, competition with fragmentation of Li^+(Lys) using Li^+(Lys)-NH_3 to describe all competing channels is included, otherwise the threshold energies nearly double. It can be noted that the experimental value obtained here is comparable to that for Li^+ bound to 12-crown-4 (12C4), 372 ± 51 kJ/mol.[101] Given that 12C4 is tetradentate, its seems odd that the tridentate Lys would have a similar bond energy, although the flexibility of the Lys side-chain allows more optimal binding of Li^+ to the N_ε amine, whereas the cyclic 12C4 ligand is more constrained in its orientation when binding Li^+. It is certainly possible that the competition with other primary decomposition channels (not accounted for here) influences the threshold for Li^+ + Lys production or that the competition is not adequately handled using the statistical treatment.[81] In particular, this method was developed and refined for competition between channels much closer in energy and the large difference in the thresholds for the deamination and Li^+ + Lys channels could lead to a breakdown in these assumptions, e.g., because anharmonicities increase the number of available states for the lower channel, which would lead to a larger kinetic shift in the Li^+ channel. Another possibility is a dynamic issue, namely at the high energies needed to induce efficient dissociation to Li^+ + Lys (more than 2 eV higher than the thermodynamic threshold, Figure 4a), the system no longer has time to explore phase space and thus dissociates diabatically to a Lys conformer more similar to that in the Li^+(Lys) complex. Formation of such a compact conformer would lead to a larger kinetic shift (and lower thermodynamic threshold) as

well. Because of these uncertainties, we believe the 376 ± 30 kJ/mol value is most conservatively viewed as an upper limit.

B3LYP, B3P86, and MP2 (with and without counterpoise corrections) all accurately predict the TCID BDEs of Na^+(Lys) with the extended neutral (219 ± 13 kJ/mol) but not with the compact neutral (201 ± 12 kJ/mol), except MP2. Previous evaluations of sodium cation affinities calculated at similar levels of theory (same single point energy level, including counterpoise corrections) find that B3LYP values tend to be high (by 8 ± 6 kJ/mol) whereas B3P86 and MP2 levels yield better agreement (mean deviations of 4 ± 5 and 2 ± 6, respectively).[102] These conclusions are consistent with the relative values found here as well.

The average TCID BDE of K^+(Lys), 160 ± 10 kJ/mol when analyzed using the extended neutral, is predicted within experimental uncertainty by all levels of theory and both basis sets, with or without counterpoise corrections on MP2. The average experimental value obtained using the compact neutral product (148 ± 12 kJ/mol) is lower than all theoretical predictions, but within experimental uncertainty for most values. Likewise, all three levels of theory provide BDEs within experimental uncertainty of the TCID values for Rb^+(Lys) and Cs^+(Lys) when interpreted using the extended neutral, 141 ± 6 and 128 ± 4 kJ/mol, respectively. In contrast, the agreement is much worse for the values obtained using the compact neutral, outside of experimental uncertainty for all but the B3LYP/def2 values.

Excluding the Li^+(Lys) results, the mean absolute deviations (MADs) of theory from experimental values with the extended neutral are about 4 kJ/mol, and 10 – 14 kJ/mol with the compact neutral. This comparison bolsters our conclusion that the analysis using the extended conformer as the neutral product for all M^+(Lys) complexes provides the most accurate BDEs, as independently concluded from the entropic effects above. If we include the Li^+(Lys) results, the MADs increase to 18 – 23 kJ/mol (extended neutral) and 9 – 14 kJ/mol (compact neutral). As noted above, difficulties in the interpretation of the Li^+(Lys) CID channel limit any conclusions that can be drawn from these values.[35,37,103-104]

4.2. Trends in Bond Energies: Metal Cation Identity and Side-Chain Substituent Effects.

The functional groups of amino acids solvate the charge of metal cations by electrostatic forces, including ion induced-dipole, ion-quadrupole, and ion-dipole forces. As for all other AAs, experimental results for the M^+(Lys) BDEs follow a trend of $Li^+ > Na^+ > K^+ > Rb^+ > Cs^+$.[23-25,28-29,32-33,35-37] Because the radii of the metal cations increases from Li^+ to Cs^+ (0.70, 0.98, 1.33, 1.49, and 1.69 Å, respectively[105]), the bond distances necessarily increase leading to reduced electrostatic interactions. As shown in Figure 6, this increase is approximately linear as the inverse of the ionic radius, as has also been demonstrated for other amino acids as well.[23,32-33,36] (Although this dependence could imply a long-range Coulombic potential, the true interactions must be superpositions of ion-dipole (r^{-2}), ion-quadrupole (r^{-3}), and ion-induced dipole (r^{-4}) forces coupled with complex chelation effects that become influential at the shorter bond distances associated with these complexes. Because the BDEs are not necessarily good reflections of the long-range potentials, plots of the BDEs versus r^{-2} and r^{-4} are no longer linear.) The lines shown in Figure 6 are linear regression fits (constrained to pass through the origin but ignoring the value for Li^+(Lys)) for the Gly, Pro, and Lys data. Slopes for the Gly, Pro, and Lys complexes are 158 ± 6, 190 ± 6, and 214 ± 6, Å kJ/mol, respectively, where the latter value matches that previously determined for Gln.[26] Clearly the point for Li^+(Lys) lies well off of the linear regression line for the other four metal cations, consistent with this value being too high. This projection indicates that a more likely value for $D_0(Li^+\text{-Lys})$ is 305 ± 9 kJ/mol, a value that agrees well with theoretical predictions as well, Table 5.

4.3. Trends in Bond Energies: Effects of Polarizability and Side Chain on M^+(AA) BDEs

We have previously found a correlation between the polarizabilities of the amino acids Gly, Met, Phe, Tyr, and Trp and their BDEs to Na^+, K^+, Rb^+, and Cs^+.[23,36-37,103] (All isotropic molecular polarizabilities used here were calculated at the PBE0/6-311+G(2d,2p) level of theory using the B3LYP/6-311G(d,p) optimized geometries of the neutral amino acid in the metal cationized complexes. This level of theory has been shown to provide polarizabilities that are in

good agreement with measured values.[106]) The polarizability correlation established by these five amino acids permits the enhanced binding observed for polar side chains to be assessed more quantitatively.[24-26,33,39] For Na^+ - Cs^+, Ser, Thr, Asp, Asn, Glu, Gln, and His all show enhanced binding compared to values predicted from the polarizability correlation. For Na^+ and K^+, BDEs to Ser, Thr, Asn, Gln, and His form a series that is parallel to those for the aliphatic amino acids, with an average enhancement of approximately 28 and 24 kJ/mol, respectively.[33,35] Asp and Glu form a separate series in between the polar and aliphatic series (enhancements of about 15 kJ/mol for both Na^+ and K^+), consistent with the reduced binding for the carboxylic acid side-chain relative to a carboxamide side chain, a result of the inductive effect of the hydroxyl group. For Rb^+, a similar trend is observed but here the enhancement is only 5 – 7 kJ/mol for Ser and Thr,[29,32] ~ 15 kJ/mol for Asp, Glu, and His,[33] and Asn and Gln form a series about 24 kJ/mol above the polarizability trend.[26] For Cs^+, Ser and Thr lie ~7 kJ/mol above the trend line;[29,32] Asp, Glu, and His average about 10 kJ/mol above the polarizability trend,[33] with Asn ~15 kJ/mol above and Gln ~24 kJ/mol higher. Thus, the shorter polar side chains of Ser and Thr (only two atoms long) drop from 28 to 24 to 10 to 7 kJ/mol in going from Na^+ to K^+ to Rb^+ to Cs^+, a result of the larger metal cation radius not being able to bind as efficiently in a tridentate conformation as smaller cations.[29,32] For Asp (three atom side chain), Glu (four atom side chain), and His (three atom side chain), the enhancements drop from 28 (Na^+) to 24 (K^+) to 15 (Rb^+) and 15 (Cs^+) kJ/mol, demonstrating better tridentate binding than the short side chain AAs. Asn/Gln (3/4 atom carboxamide side chain) show trends of 28/28 (Na^+), 24/24 (K^+), 24/24 (Rb^+) and 15/24 (Cs^+) kJ/mol. Thus, the long side chain length and strongly binding carbonyl group of the carboxamide makes the enhancement largely independent of metal for Gln and nearly so for Asn.

The five atom side chain length of Lys presumably allows facile orientation of the side chain such that the amine group can bind efficiently to a metal ion of any size. Indeed, we find that the enhancement for Lys relative to the polarizability trend is 25 (Na^+), 18 (K^+), 20 (Rb^+), and 21 (Cs^+) kJ/mol, similar to the results for Gln although about 4 kJ/mol weaker for all metal cations. Given that the local dipole moment of the carboxamide group (estimated from

acetamide, 3.68 D) is much larger than that for the amine (estimated from methyl amine, 1.31 D),[107] it is clear that the flexible lysine side-chain allows binding at close to an optimum distance and orientation, whereas the shorter side-chain length of Gln leads to constraints.

4.4. Potential complexation motifs in peptides and proteins

Under normal physiological and aqueous conditions (pH < 10), the side chain of lysine (as an AA or in a peptide) would be protonated. However, metal ligation of the side chain could be competitive under some circumstances, including higher pH conditions. Section 3.2 and the Supporting Information identified the ground and low-energy conformers of M^+(Lys), respectively. Of the eighteen structural motifs located here for the M^+(Lys) complexes, six of these are available in peptides and proteins: [N_α,N_ε,CO], [N_α,N_ε], [N_α,CO], [N_ε,CO], [CO]$^{\alpha 2}$, and [CO]$^\beta$. In five of these low-energy motifs ([N_α,N_ε,CO], [N_α,CO], [N_ε,CO], [CO]$^{\alpha 2}$, and [CO]$^\beta$), the hydroxyl moiety contributes to M^+(Lys) stabilization via hydrogen bonding to lower the relative energy. The exception is [N_α,N_ε], where the hydroxyl moiety cannot stabilize the conformer.

With [N_α,N_ε,CO] conformers, the N_α and carbonyl O are cis ($\angle N_\alpha C_\alpha CO$), and this is a plausible structural candidate in a peptide, as it is the facile rotation about the C_α–CO bond that allows for secondary structure in proteins. [N_α,N_ε,CO] is the only *tridentate* M^+(Lys) structure that is available for metal cation binding in peptides and proteins, and is the ground conformer for Li^+(Lys) and Na^+(Lys).

The [N_α,CO] and [N_ε,CO] structures are bidentate. [N_α,CO] would be an appropriate metal binding site along the backbone of any amino acid in a peptide or protein, with N_α and CO cis. [N_α,CO]cggggg$_+$, [N_α,CO]cctggg, and [N_α,CO]cggtgg (see Table S2) are all stabilized by H-bonding; however, in [N_α,CO]ccgtgg, there is no intramolecular stabilization. These structures have relative energies of 19, 58, 91, and 74 kJ/mol, respectively, using B3LYP. The [N_ε,CO] structures are also plausible chelation motifs of lysine moieties in peptides and proteins. In the [N_ε,CO] structures, N_α and CO are trans, which is also allowed, because the rotation about

C_α–CO is not limited.

A unique structure of M^+(Lys) is the bidentate [N_α,N_ε], which is the only low energy M^+(Lys) conformer that neither chelates the hydroxyl oxygen nor uses it to stabilize the conformer via hydrogen bonding; thus it could contribute to peptide and protein cationization. The [N_α,N_ε] structure of K^+(Lys) in Figure S2l is representative of Li^+(Lys), Na^+(Lys), and Cs^+(Lys), which differ only slightly in the first three dihedral angles. The side-chain dihedrals are consistent and visually all M^+(Lys) [N_α,N_ε] appear similar. (A Rb^+(Lys) [N_α,N_ε] structure could not be located.)

The $[CO]^{\alpha 2}$ and $[CO]^\beta$ structures are monodentate and therefore somewhat higher in relative energy. They are also appropriate candidates for M^+ binding in peptides and proteins, as the rotation about C_α–CO is not defined. Notably, these structures, along with [N_α,CO], can occur independent of the identity of the side-chain. Only [N_α,N_ε,CO], [N_α,N_ε], and [N_ε,CO] have the side chain and all or part of the backbone directly involved in metal cation binding. For these structures, one imagines that the length and flexibility of the lysine side chain could create an intramolecular "pocket" that could provide a natural proclivity for or discrimination against metal cations of particular radii.

5. CONCLUSIONS

Analysis of the TCID data for the five M^+(Lys) complexes requires molecular parameters for the likely ground structures of the complexes and the neutral Lys product. Hence the present study includes a thorough investigation of the conformers of these species. The levels of theory and basis sets used located the common tridentate ground conformer [N_α,N_ε,CO] for Li^+(Lys) and Na^+(Lys), but different ground structures for the larger metal cations. For K^+(Lys), the ground structure is $[CO_2^-]^\beta$ at B3LYP, B3P86, MP2, and B3LYP/def2 levels, whereas M06/def2 and MP2/def2 yielded [N_ε,CO(OH)], where the hydroxyl oxygen only partially solvates the metal cation compared to N_ε and the carbonyl oxygen. Likewise, for Rb^+(Lys) and Cs^+(Lys), the B3LYP/def2 ground structures were $[CO_2^-]^\beta$ and [N_ε,CO(OH)] for M06/def2 and MP2/def2.

The [N_ε,CO(OH)] ground structure located for K^+(Lys) and Cs^+(Lys), together with the companion zwitterionic [N_ε,CO_2^-] analogue (which co-exist in a double well potential, Figure S6), better explains previous IRMPD results. Although relative Gibbs energies at 298 K suggest that [N_ε,CO] and even [N_α,N_ε,CO] could also be contributing to the nonspecific nonzwitterionic species in the IRMPD spectra, they are not necessary to explain the observed spectra.

In addition to these ground conformations, annealing, metal cation substitution, companion NZ-ZW and transition state searches yielded a plethora of low-energy structures, including the novel $[CO]^{\beta}$, $[CO]^{\alpha 2}$, and [N_α,N_ε] binding motifs. [N_α,N_ε,CO], [N_ε,CO], and [N_α,N_ε] are among the physiologically relevant structures that could be found in protein and peptide structures.

Computational results for neutral lysine yielded four different possible ground structures, with an extended [OH-O-H_2N_α]tgtttt$_+$ and a more compact [OH-N_ε,CO-H_2N_α]cggggg$_-$ structure being low lying at all levels of theory. When modeling the TCID data for reaction 4 with M^+ = Na^+, K^+, Rb^+, and Cs^+, it was shown that formation of the extended neutral product (least constrained by hydrogen bonding) was strongly favored entropically, even if the more compact structure was lower in energy.

Experimental BDEs for M^+(Lys) extracted from modeling the TCID cross sections as dissociating to the extended conformer are in very good agreement with theoretical values for M^+ = Na^+, K^+, Rb^+, and Cs^+ within experimental error. For Li^+(Lys), modeling the data with the compact conformer led to a BDE in better agreement with theory, but competition with much lower energy channels ($N_\varepsilon H_3$ loss) or dynamic effects could explain the elevated threshold found for TCID of Li^+(Lys) to the extended conformer. The BDE trend for these Group 1 metal ions to lysine follows the usual trend of Li^+(Lys) > Na^+(Lys) > K^+(Lys) > Rb^+(Lys) > Cs^+(Lys), exhibiting an inverse dependence on the metal cation radius. The binding of Lys to the Group 1 metal cations is enhanced compared to amino acids without polar side chains by about 20 kJ/mol for all metals, a consequence of the flexibility of the Lys side chain, which permits optimal orientation and distance to the metal cation.

ASSOCIATED CONTENT

Supporting Information

The Supporting Information is available free of charge on the ACS Publications website at DOI: 10.1021/acs.jpcb.xxxxx

AUTHOR INFORMATION

*Corresponding Author; *E-mail: armentrout@chem.utah.edu.

ORCID

M. T. Rodgers: 0000-0002-5614-0948

P. B. Armentrout: 0000-0003-2953-6039

Notes

The authors declare no competing financial interest.

ACKNOWLEDGMENTS

Financial support was provided by the National Science Foundation, Grants No. CHE-1664618 (PBA) and DBI-0922819 and CHE-1709789 (MTR). In addition, we thank the Center for High Performance Computing at the University of Utah for the generous allocation of computer time. We thank Profs. M. F. Bush and E. R. Williams for providing us their K^+(Lys) and Cs^+(Lys) IRMPD spectra and structural information.

REFERENCES

1. Susa, A. C.; Mortensen, D. N.; Williams, E. R., Effects of Cations on Protein and Peptide Charging in Electrospray Ionization from Aqueous Solutions. *J. Am. Soc. Mass. Spectrom.* **2014,** *25*, 918-927.

2. Zarse, K.; Terao, T.; Tian, J.; Iwata, N.; Ishii, N.; Ristow, M., Low-Dose Lithium Uptake Promotes Longevity in Humans and Metazoans. *Eur. J. Nutr.* **2011,** *50*, 387-9.

3. Forlenza, O. V.; Paula, V. J. d.; Machado-Vieira, R.; Diniz, B. S.; Gattaz, W. F., Does Lithium Prevent Alzheimer's Disease? *Drugs & Aging* **2012,** *29*, 335-42.

4. Grof, P.; Müller-Oerlinghausen, B., A Critical Appraisal of Lithium's Efficacy and Effectiveness: The Last 60 Years. *Bipolar Disord.* **2009,** *11*, 10-19.

5. Yatham, L. N.; Kennedy, S. H.; Schaffer, A.; Parikh, S. V.; Beaulieu, S.; O'Donovan, C.; MacQueen, G.; McIntyre, R. S.; Sharma, V., et al., Canadian Network for Mood and Anxiety Treatments (CANMAT) and International Society for Bipolar Disorders (ISBD) Collaborative Update of CANMAT Guidelines for the Management of Patients with Bipolar Disorder: Update 2009. *Bipolar Disord.* **2009,** *11*, 225-255.

6. Jermain, D.; Crismon, M.; Martin, E., Population Pharmacokinetics of Lithium. *Clin. Pharm.* **1991,** *10*, 376-381.

7. Spirtes, M. A., Lithium Levels in Monkey and Human Brain after Chronic, Therapeutic, Oral Dosage. *Pharmacol. Biochem. Behav.* **1976,** *5*, 143-7.

8. Pandey, G. N.; Sarkadi, B.; Haas, M.; Gunn, R. B.; Davis, J. M.; Tosteson, D. C., Lithium Transport Pathways in Human Red Blood Cells. *J. Gen. Physiol.* **1978,** *72*, 233-247.

9. Mendlewicz, J.; Verbanck, P.; Linkowski, P.; Wilmotte, J., Lithium Accumulation in Erythrocytes of Manic-Depressive Patients: An *in Vivo* Twin Study. *Br. J. Psychiatry* **1978,** *133*, 436-44.

10. Schuermann, W. "Lithium in the Brain." *ScienceDaily* [Online]. Munich, 2013, <www.sciencedaily.com/releases/2013/09/130926103031.htm>. (accessed 26 September 2013).

11. Lichtinger, J.; Gernhäuser, R.; Bauer, A.; Bendel, M.; Canella, L.; Graw, M.; Krücken, R.; Kudejova, P.; Mützel, E., et al., Position Sensitive Measurement of Lithium Traces in Brain Tissue with Neutrons. *Med. Phys.* **2013,** *40*, 023501-1-8.

12. Timmer, R. T.; Sands, J. M., Lithium Intoxication. *J. Am. Soc. Nephrol.* **1999,** *10*, 666-74.

13. Saha, G. B.; MacIntyre, W. J.; Go, R. T., Cyclotrons and Positron Emission Tomography Radiopharmaceuticals for Clinical Imaging. *Seminars in Nuclear Medicine* **1992,** *22* 150 - 161.

14. Yen, C. K.; Budinger, T. F., Evaluation of Blood-Brain Barrier Permeability Changes in Rhesus Monkeys and Man Using ^{82}Rb and Positron Emission Tomography. *J. Comp. Assist. Tomog.* **1981,** *5*, 792-799.

15. Lam, Y. L.; Zeng, W.; Sauer, D. B.; Jiang, Y., The Conserved Potassium Channel Filter Can Have Distinct Ion Binding Profiles: Structural Analysis of Rubidium, Cesium, and Barium

Binding in NaK2K. *J. Gen. Physiol.* **2014,** *144*, 181–192.

16. Love, W. D.; Ishihara, Y.; Lyon, L. D.; Smith, R. O., Differences in the Relationships between Coronary Blood Flow and Myocardial Clearance of Isotopes of Potassium, Rubidium, and Cesium. *Am. Heart J.* **1968,** *76*, 353 - 355.

17. Yablokov, A. V.; Nesterenko, V. B.; Nesterenko, A. V.; Sherman-Nevinger, J. D., Chernobyl: Consequences of the Catastrophe for People and the Environment. *Ann. N.Y. Acad. Sci.* **2009,** *1181*, 1-335.

18. Hirose, K., Fukushima Daiichi Nuclear Plant Accident: Atmospheric and Oceanic Impacts over the Five Years. *J. Environ. Radioact.* **2016,** *157*, 113-130.

19. Gal, J.-F.; Maria, P.-C.; Massi, L.; Mayeux, C.; Burk, P.; Tammiku-Taul, J., Cesium Cation Affinities and Basicities. *Int. J. Mass Spectrom.* **2007,** *267*, 7-23.

20. Mayeux, C.; Tammiku-Taul, J.; Massi, L.; Lohu, E.-L.; Burk, P.; Maria, P.-C.; Gal, J.-F., Interaction of the Cesium Cation with Mono-, Di-, and Tricarboxylic Acids in the Gas Phase. A Cs^+ Affinity Scale for Cesium Carboxylates Ion Pairs. *J. Am. Soc. Mass. Spectrom.* **2009,** *20*, 1912-1924.

21. Bandazhevsky, Y. I., *Radioactive Cesium and the Heart: Pathophysiological Aspects*. "The Belrad Institute": Minsk, 2001; p 64.

22. Rodgers, M. T.; Armentrout, P. B., Cationic Noncovalent Interactions: Energetics and Periodic Trends. *Chem. Rev.* **2016,** *116*, 5642–5687

23. Rodgers, M. T.; Armentrout, P. B., Discriminating Properties of Metal Alkali Ions Towards the Constituents of Proteins and Nucleic Acids. Conclusions from Gas-Phase and Theoretical Studies. In *Metal Ions in Life Sciences. Volume 16: The Alkali Metal Ions: Their Role for Life*, Sigel, A.; Sigel, H.; O., Siegel, R. K., Eds. Springer: Cham, Switzerland, 2016; pp 103-131.

24. Heaton, A. L.; Moision, R. M.; Armentrout, P. B., Experimental and Theoretical Studies of Sodium Cation Interactions with the Acidic Amino Acids and Their Amide Derivatives. *J. Phys. Chem. A* **2008,** *112*, 3319-3327.

25. Heaton, A. L.; Armentrout, P. B., Experimental and Theoretical Studies of Potassium Cation Interactions with the Acidic Amino Acids and Their Amide Derivatives. *J. Phys. Chem. B* **2008,** *112*, 12056–12065.

26. Armentrout, P. B.; Yang, B.; Rodgers, M. T., Metal Cation Dependence of Interactions with Amino Acids: Bond Dissociation Energies of Rb^+ and Cs^+ to the Acidic Amino Acids and Their

Amide Derivatives. *J. Phys. Chem. B* **2014,** *118*, 4300–4314.

27. Armentrout, P. B.; Ye, S. J.; Gabriel, A.; Moision, R. M., Energetics and Mechanism for the Deamination of Lithiated Cysteine. *J. Phys. Chem. B* **2010,** *114*, 3938–3949.

28. Armentrout, P. B.; Armentrout, E. I.; Clark, A. A.; Cooper, T. E.; Stennett, E. M. S.; Carl, D. R., An Experimental and Theoretical Study of Alkali Metal Cation Interactions with Cysteine. *J. Phys. Chem. B* **2010,** *114*, 3927–3937.

29. Armentrout, P. B.; Chen, Y.; Rodgers, M. T., Metal Cation Dependence of Interactions with Amino Acids: Bond Energies of Cs^+ to Gly, Pro, Ser, Thr, and Cys. *J. Phys. Chem. A* **2012,** *116*, 3989-3999.

30. Moision, R. M.; Armentrout, P. B., An Experimental and Theoretical Dissection of Sodium Cation/Glycine Interactions. *J. Phys. Chem. A* **2002,** *106*, 10350-10362.

31. Rodgers, M. T.; Armentrout, P. B., A Critical Evaluation of the Experimental and Theoretical Determination of Lithium Cation Affinities. *Int. J. Mass Spectrom.* **2007,** *267*, 167-182.

32. Bowman, V. N.; Heaton, A. L.; Armentrout, P. B., Metal Cation Dependence of Interactions with Amino Acids: Bond Energies of Rb^+ to Gly, Ser, Thr, and Pro. *J. Phys. Chem. B* **2010,** *114*, 4107-4114.

33. Armentrout, P. B.; Citir, M.; Chen, Y.; Rodgers, M. T., Thermochemistry of Alkali Metal Cation Interactions with Histidine: Influence of the Side-Chain. *J. Phys. Chem. A* **2012,** *116*, 11823-11832.

34. Shoeib, T.; Zhao, J.; Aribi, H. E.; Hopkinson, A. C.; Siu, K. W. M., Dissociations of Complexes between Monovalent Metal Ions and Aromatic Amino Acid or Histidine. *J. Am. Soc. Mass. Spectrom.* **2013,** *24*, 38-48.

35. Armentrout, P. B.; Gabriel, A.; Moision, R. M., An Experimental and Theoretical Study of Alkali Metal Cation/Methionine Interactions. *Int. J. Mass Spectrom.* **2009,** *283*, 56-68.

36. Armentrout, P. B.; Yang, B.; Rodgers, M. T., Metal Cation Dependence of Interactions with Amino Acids: Bond Energies of Rb^+ and Cs^+ to Met, Phe, Tyr, and Trp. *J. Phys. Chem. A* **2013,** *117*, 3771-3781.

37. Ruan, C.; Rodgers, M. T., Cation-Π Interactions: Structures and Energetics of Complexation of Na^+ and K^+ with the Aromatic Amino Acids, Phenylalanine, Tyrosine and Tryptophan. *J. Am. Chem. Soc.* **2004,** *126*, 14600-14610.

38. Moision, R. M.; Armentrout, P. B., The Special Five-Membered Ring of Proline: An Experimental and Theoretical Investigation of Alkali Metal Cation Interactions with Proline and Its Four- and Six-Membered Ring Analogues. *J. Phys. Chem. A* **2006,** *110*, 3933-3946.

39. Ye, S. J.; Clark, A. A.; Armentrout, P. B., An Experimental and Theoretical Investigation of Alkali Metal Cation Interactions with Hydroxyl Side Chain Amino Acids. *J. Phys. Chem. B* **2008,** *112*, 10291-10302.

40. Forbes, M. W.; Bush, M. F.; Polfer, N. C.; Oomens, J.; Dunbar, R. C.; Williams, E. R.; Jockusch, R. A., Infrared Spectroscopy of Arginine Cation Complexes: Direct Observation of Gas-Phase Zwitterions. *J. Phys. Chem. A* **2007,** *111*, 11759-11770.

41. Bush, M. F.; O'Brien, J. T.; Prell, J. S.; Saykally, R. J.; Williams, E. R., Infrared Spectroscopy of Cationized Arginine in the Gas Phase: Direct Evidence for the Transition from Nonzwitterionic to Zwitterionic Structure. *J. Am. Chem. Soc.* **2007,** *129*, 1612-1622.

42. Heaton, A. L.; Bowman, V. N.; Oomens, J.; Steill, J. D.; Armentrout, P. B., Infrared Multiple Photon Dissociation Spectroscopy of Cationized Asparagine: Effects of Metal Cation Size on Gas-Phase Conformation. *J. Phys. Chem. A* **2009,** *113*, 5519-5530.

43. O'Brien, J. T.; Prell, J. S.; Steill, J. D.; Oomens, J.; Williams, E. R., Interactions of Mono- and Divalent Metal Ions with Aspartic and Glutamic Acid Investigated with IR Photodissociation Spectroscopy and Theory. *J. Phys. Chem. A* **2008,** *112*, 10823-10830.

44. Citir, M.; Stennett, E. M. S.; Oomens, J.; Steill, J. D.; Rodgers, M. T.; Armentrout, P. B., Infrared Multiple Photon Dissociation Spectroscopy of Cationized Cysteine: Effects of Metal Cation Size on Gas-Phase Conformation. *Int. J. Mass Spectrom.* **2010,** *297*, 9-17.

45. Bush, M. F.; Oomens, J.; Saykally, R. J.; Williams, E. R., Alkali Metal Ion Binding to Glutamine and Glutamine Derivatives Investigated by Infrared Action Spectroscopy and Theory. *J. Phys. Chem. A* **2008,** *112*, 8578-8584.

46. Kapota, C.; Lemaire, J.; Maitre, P.; Ohanessian, G., Vibrational Signature of Charge Solvation Vs Salt Bridge Isomers of Sodiated Amino Acids in the Gas Phase. *J. Am. Chem. Soc.* **2004,** *126*, 1836-1842.

47. Citir, M.; Hinton, C. S.; Oomens, J.; Steill, J. D.; Armentrout, P. B., Infrared Multiple Photon Dissociation Spectroscopy of Cationized Histidine: Effects of Metal Cation Size on Gas-Phase Conformation. *J. Phys. Chem. A* **2012,** *116*, 1532-1541.

48. Bush, M. F.; Forbes, M. W.; Jockusch, R. A.; Oomens, J.; Polfer, N. C.; Saykally, R. J.;

Williams, E. R., Infrared Spectroscopy of Cationized Lysine and ε-N-Methyllysine in the Gas Phase: Effects of Alkali-Metal Ion Size and Proton Affinity on Zwitterion Stability. *J. Phys. Chem. A* **2007,** *111*, 7753-7760.

49. Bush, M. F.; Oomens, J.; Williams, E. R., Proton Affinity and Zwitterion Stability: New Results from Infrared Spectroscopy and Theory of Cationized Lysine and Analogues in the Gas Phase. *J. Phys Chem. A* **2009,** *113*, 431-438.

50. Carl, D. R.; Cooper, T. E.; Oomens, J.; Steill, J. D.; Armentrout, P. B., Infrared Multiple Photon Dissociation Spectroscopy of Cationized Methionine: Effects of Alkali-Metal Cation Size on Gas-Phase Conformation. *Phys. Chem. Chem. Phys.* **2010,** *12*, 3384-3398.

51. Polfer, N. C.; Paizs, B.; Snoek, L. C.; Compagnon, I.; Suhai, S.; Meijer, G.; von Helden, G.; Oomens, J., Infrared Fingerprint Spectroscopy and Theoretical Studies of Potassium Ion Tagged Amino Acids and Peptides in the Gas Phase. *J. Am. Chem. Soc.* **2005,** *127*, 8571-8579.

52. Dunbar, R. C.; Steill, J. D.; Oomens, J., Cationized Phenylalanine Conformations Characterized by IRMPD and Computation for Singly and Doubly Charged Ions. *Phys. Chem. Chem. Phys.* **2010,** *12*, 13383-13393.

53. Drayss, M. K.; Blunk, D.; Oomens, J.; Schäfer, M., Infrared Multiple Photon Dissociation Spectroscopy of Potassiated Proline. *J. Phys Chem. A* **2008,** *112*, 11972-11974.

54. Drayss, M. K.; Armentrout, P. B.; Oomens, J.; Schäfer, M., IR Spectroscopy of Cationized Aliphatic Amino Acids: Stability of Charge-Solvated Structure Increases with Metal Cation Size. *Int. J. Mass Spectrom.* **2010,** *297*, 18–27.

55. Armentrout, P. B.; Rodgers, M. T.; Oomens, J.; Steill, J. D., Infrared Multiphoton Dissociation Spectroscopy of Cationized Serine: Effects of Alkali-Metal Cation Size on Gas-Phase Conformation. *J. Phys. Chem. A* **2008,** *112*, 2248-2257.

56. Rodgers, M. T.; Armentrout, P. B.; Oomens, J.; Steill, J. D., Infrared Multiphoton Dissociation Spectroscopy of Cationized Threonine: Effects of Alkali-Metal Cation Size on Gas-Phase Conformation. *J. Phys. Chem. A* **2008,** *112*, 2258-2267.

57. Polfer, N. C.; Oomens, J.; Dunbar, R. C., IRMPD Spectroscopy of Metal-Ion/Tryptophan Complexes. *Phys. Chem. Chem. Phys.* **2006,** *8*, 2744-2751.

58. Heaton, A. L.; Armentrout, P. B., Thermodynamics and Mechanism of the Deamidation of Sodium-Bound Asparagine. *J. Am. Chem. Soc.* **2008,** *130*, 10227-10232.

59. Mookherjee, A.; Armentrout, P. B., Theoretical Investigation and Reinterpretation of the

Decomposition of Lithiated Proline and N-Methyl Proline. *Int. J. Mass Spectrom.* **2014,** *370*, 16-28.

60. Ye, S. J.; Armentrout, P. B., An Experimental and Theoretical Investigation of the Decomposition of Lithiated Hydroxyl Side Chain Amino Acids. *J. Phys. Chem. B* **2008,** *112*, 10303-10313.

61. Dookeran, N. N.; Yalcin, T.; Harrison, A. G., Fragmentation Reactions of Protonated α-Amino Acids. *J. Mass Spectrometry* **1996,** *31*, 500-508.

62. Milne, G. W. A.; Axenrod, T.; Fales, H. M., Chemical Ionization Mass Spectrometry of Complex Molecules. IV. Amino Acids. *J. Am. Chem. Soc.* **1970,** *92*, 5170-5175.

63. Moision, R. M.; Armentrout, P. B., An Electrospray Ionization Source for Thermochemical Investigation with the Guided Ion Beam Mass Spectrometer. *J. Am. Soc. Mass Spectrom.* **2007,** *18*, 1124-1134.

64. Ervin, K. M.; Armentrout, P. B., Translational Energy Dependence of $Ar^+ + XY \rightarrow ArX^+ + Y$ ($XY = H_2, D_2$, HD from Thermal to 30 eV C.M. *J. Chem. Phys.* **1985,** *83*, 166-189.

65. Muntean, F.; Armentrout, P. B., Guided Ion Beam Study of Collision-Induced Dissociation Dynamics: Integral and Differential Cross Sections. *J. Chem. Phys.* **2001,** *115*, 1213-1228.

66. Rodgers, M. T., Substituent Effects in the Binding of Alkali Metal Ions to Pyridines Studied by Threshold Collision-Induced Dissociation and Ab Initio Theory: The Methylpyridines. *J. Phys. Chem. A* **2001,** *105*, 2374-2383.

67. Kim, T.; Tolmachev, A. V.; Harkewicz, R.; Prior, D. C.; Anderson, G.; Udseth, H. R.; Smith, R. D.; Bailey, T. H.; Rakov, S., et al., Design and Implementation of a New Electrodynamic Ion Funnel. *Anal. Chem* **2000,** *72*, 2247-2255.

68. Ye, S. J.; Armentrout, P. B., Absolute Thermodynamic Measurements of Alkali Metal Cation Interactions with a Simple Dipeptide and Tripeptide. *J. Phys. Chem. A* **2008,** *112*, 3587-3596.

69. Carl, D. R.; Moision, R. M.; Armentrout, P. B., Binding Energies for the Inner Hydration Shells of Ca^{2+}: An Experimental and Theoretical Investigation of $Ca^{2+}(H_2O)x$ Complexes ($x = 5 – 9$). *Int. J. Mass Spectrom.* **2007,** *265*, 308-325.

70. Carpenter, J. E.; McNary, C. P.; Furin, A.; Sweeney, A. F.; Armentrout, P. B., How Hot Are Your Ions Really? A Threshold Collision-Induced Dissociation Study of Substituted Benzylpyridinium "Thermometer" Ions. *J. Am. Soc. Mass Spectrom.* **2017**, 1-13.

71. Gerlich, D., Inhomogeneous rf Fields: A Versatile Tool for the Study of Processes with Slow Ions. *Adv. Chem. Phys.* **1992,** *82*, 1-176.

72. Aristov, N.; Armentrout, P. B., Collision-Induced Dissociation of Vanadium Monoxide Ion. *J. Phys. Chem.* **1986,** *90*, 5135-5140.

73. Hales, D. A.; Armentrout, P. B., Effect of Internal Excitation on the Collision-Induced Dissociation and Reactivity of Co_2^+. *J. Cluster Science* **1990,** *1*, 127-142.

74. Hales, D. A.; Lian, L.; Armentrout, P. B., Collision-Induced Dissociation of Nb_n^+ (n = 2 - 11): Bond Energies and Dissociation Pathways. *Int. J. Mass Spectrom. Ion Processes* **1990,** *102*, 269-301.

75. Daly, N. R., Scintillation Type Mass Spectrometer Ion Detector. *Rev. Sci. Instrum.* **1960,** *31*, 264-267.

76. Chantry, P. J., Doppler Broadening in Beam Experiments. *J. Chem. Phys.* **1971,** *55*, 2746-2759.

77. Gilbert, R. G.; Smith, S. C., *Theory of Unimolecular and Recombination Reactions*. Blackwell Scientific: London, 1990.

78. Truhlar, D. G.; Garrett, B. C.; Klippenstein, S. J., Current Status of Transition-State Theory. *J. Phys. Chem.* **1996,** *100*, 12771-12800.

79. Holbrook, K. A.; Pilling, M. J.; Robertson, S. H., *Unimolecular Reactions*. 2nd ed.; Wiley: New York, 1996.

80. Rodgers, M. T.; Ervin, K. M.; Armentrout, P. B., Statistical Modeling of Collision-Induced Dissociation Thresholds. *J. Chem. Phys.* **1997,** *106*, 4499-4508.

81. Rodgers, M. T.; Armentrout, P. B., Statistical Modeling of Competitive Threshold Collision-Induced Dissociation. *J. Chem. Phys.* **1998,** *109*, 1787-1800.

82. Beyer, T. S.; Swinehart, D. F., Number of Multiply-Restricted Partitions. *Commun. ACM* **1973,** *16*, 379.

83. Stein, S. E.; Rabinovich, B. S., On the Use of Exact State Counting Methods in RRKM Rate Calculations. *Chem. Phys. Lett.* **1977,** *49*, 183-188.

84. Pearlman, D. A.; Case, D. A.; Caldwell, J. W.; Ross, W. R.; Cheatham, T. E.; DeBolt, S.; Ferguson, D.; Seibel, G.; Kollman, P., Amber, a Computer Program for Applying Molecular Mechanics, Normal Mode Analysis, Molecular Dynamics and Free Energy Calculations to Elucidate the Structures and Energies of Molecules. *Comp. Phys. Commun.* **1995,** *91*, 1-41.

85. Boeckx, B.; Maes, G., Experimental and Theoretical Observation of Different Intramolecular H-Bonds in Lysine Conformations. *J. Phys. Chem. B* **2012,** *116*, 12441-12449.

86. Leng, Y.; Zhang, M.; Song, C.; Chen, M.; Lin, Z., A Semi-Empirical and Ab Initio Combined Approach for the Full Conformational Searches of Gaseous Lysine and Lysine–H_2O Complex. *J. Mol. Struct. (Theochem)* **2008,** *858*, 52-65.

87. Frisch, M. J.; Trucks, G. W.; Schlegel, H. B.; Scuseria, G. E.; Robb, M. A.; Cheeseman, J. R.; Scalmani, G.; Barone, V.; Mennucci, B., et al. *Gaussian 09, Revision D.01* Gaussian, Inc.: Wallingford, CT, USA, 2009.

88. Woon, D. E.; Dunning, T. H., Jr., Gaussian Basis Sets for Use in Correlated Molecular Calculations. V. Core-Valence Basis Sets for Boron through Neon. *J. Chem. Phys.* **1995,** *103*, 4572-4585.

89. Armentrout, P. B.; Austin, C. A.; Rodgers, M. T., Alkali Metal Cation Interactions with 12-Crown-4 in the Gas Phase: Revisited. *Int. J. Mass Spectrom.* **2012,** *330-332*, 16-26.

90. Zhao, Y.; Truhlar, D. G., The M06 Suite of Density Functionals for Main Group Thermochemistry, Thermochemical Kinetics, Noncovalent Interactions, Excited States, and Transition Elements: Two New Functionals and Systematic Testing of Four M06-Class Functionals and 12 Other Functionals. *Theor. Chem. Acc.* **2008,** *120*, 215-241.

91. Montgomery, J. A., Jr.; Frisch, M. J.; Ochterski, J. W.; Petersson, G. A., A Complete Basis Set Model Chemistry. VI. Use of Density Functional Geometries and Frequencies. *J. Chem. Phys.* **1999,** *110*, 2822.

92. van Duijneveldt, F. B.; van Duijneveldt-van de Rijdt, J. G. C. M.; van Lenthe, J. H., State of the Art in Counterpoise Theory. *Chem. Rev.* **1994,** *94*, 1873-1885.

93. Lemoff, A. S.; Bush, M. F.; O'Brien, J. T.; Williams, E. R., Structures of Lithiated Lysine and Structural Analogues in the Gas Phase: Effects of Water and Proton Affinity on Zwitterionic Stability *J. Phys. Chem. A* **2006,** *110*, 8433-8442.

94. Boles, G. C.; Owen, C. J.; Berden, G.; Oomens, J.; Armentrout, P. B., Experimental and Theoretical Investigations of Infrared Multiple Photon Dissociation Spectra of Glutamic Acid Complexes with Zn^{2+} and Cd^{2+}. *Phys. Chem. Chem. Phys.* **2017,** *19*, 12394 - 12406.

95. Boles, G. C.; Coates, R. A.; Berden, G.; Oomens, J.; Armentrout, P. B., Experimental and Theoretical Investigations of Infrared Multiple Photon Dissociation Spectra of Asparagine Complexes with Zn^{2+} and Cd^{2+} and Their Deamidation Processes. *J. Phys. Chem. B* **2016,** *120*,

12486-12500.

96. Boles, G. C.; Coates, R. A.; Berden, G.; Oomens, J.; Armentrout, P. B., Experimental and Theoretical Investigations of Infrared Multiple Photon Dissociation Spectra of Glutamine Complexes with Zn^{2+} and Cd^{2+}. *J. Phys. Chem. B* **2015,** *119*, 11607–11617.

97. Owen, C. J.; Boles, G. C.; Berden, G.; Oomens, J.; Armentrout, P. B., Experimental and Theoretical Investigations of Infrared Multiple Photon Dissociation Spectra of Lysine Complexes with Zn^{2+} and Cd^{2+}. *Eur. J. Mass Spectrom.*, in press.

98. Yalcin, T.; Csizmadia, I. G.; Peterson, M. R.; Harrison, A. G., The Structure and Fragmentation of b_n ($n \geq 3$) Ions in Peptide Spectra. *J. Am. Soc. Mass Spectrom.* **1996,** *7*, 233-242.

99. Kish, M. M.; Ohanessian, G.; Wesdemiotis, C., The Na^+ Affinities of α-Amino Acids: Side-Chain Substituent Effects. *Int. J. Mass Spectrom.* **2003,** *227*, 509-524.

100. Wang, P.; Ohanessian, G.; Wesdemiotis, C., The Sodium Ion Affinities of Asparagine, Glutamine, Histidine and Arginine. *Int. J. Mass Spectrom.* **2008,** *269*, 34-45.

101. Ray, D.; Feller, D.; More, M. B.; Glendening, E. D.; Armentrout, P. B., Cation-Ether Complexes in the Gas Phase: Bond Dissociation Energies and Equilibrium Structures of Li^+[1,2-Dimethoxyethane]$_x$, x = 1-2, and Li^+[12-Crown-4]. *J. Phys. Chem.* **1996,** *100*, 16116-16125.

102. Armentrout, P. B.; Rodgers, M. T., An Absolute Sodium Cation Affinity Scale: Threshold Collision-Induced Dissociation Experiments and Ab Initio Theory. *J. Phys. Chem. A* **2000,** *104*, 2238-2247.

103. Rodgers, M. T.; Armentrout, P. B., A Thermodynamic "Vocabulary" for Metal Ion Interactions in Biological Systems. *Acc. Chem. Res.* **2004,** *37*, 989-998.

104. Mookherjee, A.; Armentrout, P. B., Role of Methylation on the Thermochemistry of Alkali Metal Cation Complexes of Amino Acids: N-Methyl Proline. *Int. J. Mass Spectrom.* **2013,** *345-347*, 109-119.

105. Wilson, R. G.; Brewer, G. R., *Ion Beams with Applications to Ion Implantation*. Wiley: New York, 1973.

106. Smith, S. M.; Markevitch, A. N.; Romanor, D. A.; Li, X.; Levis, R. J.; Schlegel, H. B., Static and Dynamic Polarizabilities of Conjugated Molecules and Their Cations *J. Phys. Chem. A* **2000,** *108*, 11063-11072.

107. Lide, D. R., *CRC Handbook of Chemistry and Physics*. CRC Press: Boca Raton, 2002; Vol.

83.

Table 1. Relative Single Point Energies (kJ/mol) at 0 K for Low-lying Lysine Structures[a]

this work					literature[b]		
structure	dihedrals	B3LYP	B3P86/M06	MP2(full)	structure	B3LYP	MP2
[OH-O-H_2N_α]	tgtttt$_+$	0.0, *0.1,* **0.0**	3.0, *3.3,* **5.5**	9.5, *17.2,* **9.4**	LYS14	0.0	8.2
	tgtttt-	0.4, *0.0,* **0.4**	3.4, *3.4,* **5.3**	9.2, *16.6,* **9.3**	LYS12	0.5	7.8
[OH-N_ε,CO-H_2N_α]	cggggg$_-$	3.3, *5.2,* **4.3**	0.0, *1.1,* **0.0**	0.0, *0.0,* **0.0**	LYS1	0.4, 0.0[c]	0.0, 0.0[c]
	cgtggg	4.0, *5.6*, **4.9**	1.0, *1.8,* **0.2**	1.3, *0.4,* **1.4**	LYS2	2.1	2.0
[OH-N_αH-N_ε]	cgttgg$_-$	4.9, *4.8,* **5.1**	1.1, *0.0,* **2.2**	5.4, *4.4,* **3.9**	LYS5	1.7, 1.3[c]	3.4, 4.8[c]

[a]Structures shown in Figure 1 are included. See Table S1 for a complete list of all conformers. Single point energies calculated at B3LYP, B3P86, and MP2(full)/6-311+G(2d,2p)//B3LYP/6-311+G(d,p) (normal font); B3LYP, B3P86, and MP2(full)/aug-cc-pVTZ//MP2(full)/cc-pVDZ (*italics font*); or B3LYP, M06, and MP2(full)//B3LYP/def2-TZVPPD (**bold font**) with ZPE corrections scaled by 0.989. [b] Except as noted, geometries optimized and SPE calculated at B3LYP or MP2/6-31++G(d,p) with ZPE corrections scaled by 0.97.[85] [c] Geometries optimized and ZPE corrections scaled by 0.96 calculated at B3LYP/6-311++G(d,p) level with SPEs at B3LYP and MP2/6-311G(2df,p).[86]

Table 2. Relative Single Point Energies (kJ/mol) at 0 K for Low-energy Group 1-Metal Cation Lysine Structures[a]

			this work			literature	
structure	dihedrals	M^+	B3LYP	B3P86/M06	MP2(full)	B3LYP[b,c,d]	MP2
$[N_\alpha,N_\varepsilon,CO]$	t_+gggtg	Li^+	0.0, *0.0*	0.0, *0.0*	0.0, *0.0*	0.0, 0.0, 0	0
A0[b]		Na^+	0.0	0.0	0.0	0.0, 0	0
$N_{SC}N_TO$-NZ[c,d]		K^+	8.9, **5.8**	15.7, **0.7**	3.4, **1.5**	8.0, 8	4
		Rb^+	**10.1**	**4.5**	**4.7**		
		Cs^+	**14.4**	**4.9**	**7.3**	20	7
$[N_\varepsilon,CO(OH)]$	cggggt	K^+	7.9, **4.8**	11.1, **0.0**	1.8, **0.0**	5.3, 7	1
$N_{SC}OO$-NZ[c,d]		Rb^+	**4.5**	**0.0**	**0.0**		
		Cs^+	**6.0**	**0.0**	**0.0**	7	4
$[N_\varepsilon,CO_2^-]$	cggggt	Li^+	34.3, *36.4*	29.5, *30.0*	27.4, *20.8*	36.2, 36.9, 34	27
G0[b]		Na^+	22.0	17.1	16.5	21.0, 22	13
$N_{SC}OO$-ZW[c,d]		K^+	22.9, **22.1**	24.6, **22.8**	14.6, **12.0**	22.7, 22	14
		Rb^+	**24.8**	**25.2**	**14.5**		
		Cs^+	**27.3**	**24.9**	**15.0**	27	15
$[CO_2^-]^\beta$	$cgtgg_+g$	Li^+	32.5, *34.2*	24.8, *26.1*	36.9, *32.2*		
		Na^+	9.2	1.6	13.3		
		K^+	0.0, **0.0**	0.0, **10.6**	3.00, **4.8**		
		Rb^+	**0.0**	**10.8**	**8.0**		
		Cs^+	**0.0**	**10.1**	**3.8**		
$[CO_2^-]^\beta$	cggggg	Li^+	33.3, *37.2*	24.9, *27.8*	33.1, *27.7*	34.7, 34.9, 35	33
E0[b]		Na^+	10.5	2.1	10.1	5.5, 9	12
OO^β-ZW [c,d]		K^+	1.3, **1.5**	0.7, **7.8**	0.0, **1.3**	0.0, 0	0
		Rb^+	**1.7**	**8.2**	**4.6**		
		Cs^+	**1.5**	**7.0**	**0.2**	0	0

[a] Structures shown in Figure 2 are included. Single point energies calculated at B3LYP, B3P86, and MP2(full)/6-311+G(2d,2p)//B3LYP/ 6-311+G(d,p) (normal font); B3LYP, B3P86, and MP2(full)/aug-cc-pVTZ(Li-C)//MP2(full)/cc-pVDZ(Li-C) (*italics font*); or B3LYP, M06, and MP2(full)/def2-TZVPPD//B3LYP/def2-TZVPPD (**bold font**). [b] B3LYP/ 6-31++G(d,p) optimized energies for conformers of Li^+(Lys).[93] [c] B3LYP/ 6-31++G(d,p) and LACVP ECP for K^+ optimized energies for conformers of Li^+(Lys), Na^+(Lys), and K^+(Lys).[48] [d] B3LYP or MP2/6-311++G(2d,2p)//B3LYP/6-31++G(d,p) , LACVP ECP for K^+, and CRENBL ECP for Cs^+.[49]

Table 3. Relative 298 K Gibbs Energies (kJ/mol) for the Conformers of K^+(Lys) and Cs^+(Lys)

Structure	dihedrals	K^+		Cs^+	
		This work[a]	Literature[b]	This work[a]	Literature[b]
[N_α,N_ε,CO]	t_+gggtg	10.6,[c] 17.4,[d] 3.7,[e] **9.7**,[c] **9.4**,[f] **10.2**[e]	8.0,[g] 8,[c] 4[e]	**14.7**,[c] **7.8**,[f] **10.3**[e]	15,[c] 3[e]
[N_ε,CO]	cggg$_+$t$_+$g$_+$	6.7,[c] 11.5,[d] 5.6,[e] **4.5**,[c] **9.9**,[f] **11.1**[e]	2.6,[g] 4,[c] 5[e]	**4.0**,[c] **5.6**,[f] **6.4**[e]	3,[c] 0[e]
[N_ε,CO(OH)]	cggggt	7.5,[c] 10.6,[d] 0.0,[e] **0.0**,[c] **0.0**,[f] **0.0**[e]	5.0,[g] 7,[c] 1[e]	**3.3**,[c] **0.0**,[f] **0.0**[e]	2,[c] 0[e]
[N_ε,CO_2^-]	cggggt	26.6,[c] 28.3,[d] 17.0,[e] **28.2**,[c] **33.6**,[f] **22.8**[e]	24.2,[g] 24,[c] 16[e]	**29.3**,[c] **29.5**,[f] **19.7**[e]	19,[c] 8[e]
[CO_2^-]$^\beta$	cgtgg$_+$g	0.0,[c] 0.0,[d] 1.6,[e] **2.4**,[c] **17.7**,[f] **11.9**[e]		**0.0**,[c] **12.8**,[f] **6.4**[e]	
[CO_2^-]$^\beta$	cggggg	2.7,[c] 2.1,[d] 0.02,[e] **5.2**,[c] **16.2**,[f] **9.7**[e]	0,[g] 0,[c] 0[e]	**3.2**,[c] **11.3**,[f] **4.5**[e]	0,[c] 1[e]

[a]Method/6-311+G(2d,2p)//B3LYP/6-311+G(d,p) calculations (normal font) and Method/def2-TZVPPD//B3LYP/def2-TZVPPD calculations (**bold font**). [b]Unless otherwise indicated, Method/6-311++G(2d,2p)//B3LYP/6-31++G(d,p) calculations and CRENBL ECP for Cs.[49] [c]B3LYP. [d]B3P86. [e]MP2(full). [f]M06. [g]B3LYP/6-31++G(d,p) calculations and the LACVP effective core potential for K.[48]

Table 4. Fitting Parameters of Equations 1 and 2, Threshold Energies at 0 K, and Entropies of Activation at 1000 K for CID of M^+(Lys)[a]

Reactant	M^+(Lys) structure	Products	Lys structure	σ_0[c]	n[c]	E_0 (eV) no RRKM[b]	E_0 (eV) PSL[c]	$\Delta S^{\ddagger}_{1000}$ (J/Kmol)
Li^+(Lys)[d]	$[N_\alpha,N_\varepsilon,CO]t_+gggtg$[a,g]	Li^+(Nle)+ $N_\varepsilon H_3$		19.0 (1.8)	0.6 (0.1)	3.30 (0.08)	1.40 (0.09)	-98 (2)
		Li^+ + Lys	$[OH\text{-}O\text{-}H_2N_\alpha]tgtttt_+$[e]	19.0 (1.8)	0.6 (0.1)	6.85 (0.09)	3.93 (0.11)	94 (2)
	$[N_\alpha,N_\varepsilon,CO]t_+gggtg$[f]	Li^+(Nln) + $N_\varepsilon H_3$		19.2 (1.8)	0.6 (0.1)	3.31 (0.08)	1.49 (0.09)	-84 (2)
		Li^+ + Lys	$[OH\text{-}O\text{-}H_2N_\alpha]tgtttt$[e]	19.2 (1.8)	0.6 (0.1)	6.86 (0.09)	3.86 (0.12)	91 (2)
Na^+(Lys)	$[N_\alpha,N_\varepsilon,CO]t_+gggtg$[a,g]	Na^+ + Lys	$[OH\text{-}O\text{-}H_2N_\alpha]tgtttt_+$[e]	21.3 (7.1)	1.8 (0.3)	2.94 (0.22)	2.27 (0.14)	91 (2)
K^+(Lys)	$[CO_2^-]^\beta cgtgg_+g$[a,h,i]	K^+ + Lys	$[OH\text{-}O\text{-}H_2N_\alpha]tgtttt_+$[e]	42.7 (10.8)	1.6 (0.2)	1.97 (0.10)	1.67 (0.07)	79 (2)
	$[N_\varepsilon,CO(OH)]cggggt$[j]	K^+ + Lys	$[OH\text{-}O\text{-}H_2N_\alpha]tgtttt_+$[e]	42.1 (11.9)	1.6 (0.2)	1.91 (0.11)	1.61 (0.07)	60 (2)
	$[N_\varepsilon,CO_2^-]cggggt$	K^+ + Lys	$[OH\text{-}O\text{-}H_2N_\alpha]tgtttt_+$[e]	41.2 (11.6)	1.6 (0.2)	1.90 (0.11)	1.71 (0.08)	94 (2)
Rb^+(Lys)	$[CO_2^-]^\beta cgtgg_+g$[i]	Rb^+ + Lys	$[OH\text{-}O\text{-}H_2N_\alpha]tgtttt_+$[e]	19.1 (1.8)	1.3 (0.2)	1.77 (0.07)	1.46 (0.05)	77 (2)
	$[N_\varepsilon,CO(OH)]cggggt$[j]	Rb^+ + Lys	$[OH\text{-}O\text{-}H_2N_\alpha]tgtttt_+$[e]	19.1 (1.8)	1.3 (0.2)	1.79 (0.07)	1.43 (0.05)	63 (2)
	$[N_\varepsilon,CO_2^-]cggggt$	Rb^+ + Lys	$[OH\text{-}O\text{-}H_2N_\alpha]tgtttt_+$[e]	18.9 (1.8)	1.3 (0.2)	1.77 (0.08)	1.49 (0.05)	89 (2)
Cs^+(Lys)	$[CO_2^-]^\beta cgtgg_+g$[i]	Cs^+ + Lys	$[OH\text{-}O\text{-}H_2N_\alpha]tgtttt_+$[e]	20.8 (1.7)	1.0 (0.2)	1.57 (0.08)	1.33 (0.06)	75 (2)
	$[N_\varepsilon,CO(OH)]cggggt$[j]	Cs^+ + Lys	$[OH\text{-}O\text{-}H_2N_\alpha]tgtttt_+$[e]	20.7 (1.7)	1.0 (0.2)	1.59 (0.08)	1.30 (0.06)	61 (2)
	$[N_\varepsilon,CO_2^-]cggggt$	Cs^+ + Lys	$[OH\text{-}O\text{-}H_2N_\alpha]tgtttt_+$[e]	20.5 (1.7)	0.9 (0.2)	1.58 (0.08)	1.34 (0.06)	12 (2)

[a] Modeling results use ground conformer from B3LYP/6-311+G(2d,2p)//B3LYP/6-311+G(d,p) calculations unless otherwise noted. Uncertainties are listed in parentheses. [b] Lifetime effects not included. [c] With the lifetime effect included by using a PSL TS. [d] Competitive fitting results using a tight TS for NH_3 loss for the cross section sum and a PSL TS for Li^+ cross section; see text. [e] Entropically favored neutral with extended structure. [f] MP2(full)/aug-cc-pVTZ//MP2(full)/cc-

pVDZ ground conformer. [g]B3P86 and MP2(full)/6-311+G(2d,2p)//B3LYP/6-311+G(d,p) ground conformer. [h]B3P86/6-311+G(2d,2p)//B3LYP/6-311+G(d,p) ground conformer. [i]B3LYP//B3LYP/def2-TZVPPD ground conformer. [j]M06 and MP2(full)//B3LYP/def2-TZVPPD ground conformer.

Table 5. Comparison of Experimental and Theoretical Bond Dissociation Energies (kJ/mol) of Complexes of Metalated Lysine at 0 K

product channel	TCID experiment[a]		Theory[b]		
	extended	compact	B3LYP	B3P86/M06[b]	MP2(full)
Li^+ + Lys[c]	376 ± 30	[331 ± 26]	322.6, *328.6*[c]	314.6, *320.2*[c]	306.1 (321.0), *311.3 (320.3)*[c]
Na^+ + Lys	219 ± 13	[201 ± 12]	223.6	216.6	209.2 (223.6)
K^+ + Lys	160 ± 10	[148 ± 12]	160.6, **154.6**[d]	167.0, **157.4**[d]	157.0 (162.1), **157.7 (167.0)**[d]
Rb^+ + Lys	141 ± 6	[130 ± 9]	**135.4**[d]	**143.0**[d]	**141.7 (155.6)**[d]
Cs^+ + Lys	128 ± 4	[118 ± 8]	**122.4**[d]	**132.2**[d]	**131.9 (141.1)**[d]
MAD[e]			18 ± 24 [9 ± 7]	20 ± 28 [14 ± 3]	23 ± 33 [14 ± 6]
MAD[f]			4 ± 2 [10 ± 8]	4 ± 2 [14 ± 4]	4 ± 4 [11 ± 2]

[a] Results from Table 4. [b] Energies calculated at the corresponding 6-311+G(2d,2p)//B3LYP/6-311+G(d,p) level except where noted (normal font). Zero-point energies and counterpoise corrections for BSSE are included in all theoretical BDE values with values excluding counterpoise corrections in parentheses. [c] Energies calculated at the corresponding aug-cc-pVTZ(Li-C)//MP2(full)/cc-pVDZ(Li-C) level (*italic font*). [d] Energies calculated at corresponding def2-TZVPPD//B3LYP/def2-TZVPPD level (**bold font**). [e] Mean absolute deviation (MAD) from experimental threshold energies with extended [compact] neutral including lithium. [f] MAD from experimental threshold energies with extended [compact] neutral excluding lithium.

Figure Captions

Figure 1. Ground conformers of neutral lysine optimized at the B3LYP/6-311+G(d,p) level. Dotted lines indicate hydrogen bonds. Relative 0 K energies in kJ/mol calculated at the B3LYP, M06, and MP2 levels using the def2-TZVPPD basis set are also shown with values for other levels in Table 1.

Figure 2. Ground conformers of M^+(Lys) shown as K^+(Lys). All structures are optimized at B3LYP/6-311+G(d,p) level. Dotted lines indicate hydrogen bonds and dashed lines show metal ligand interactions. Relative 298 K Gibbs energies in kJ/mol calculated at the B3LYP, M06, and MP2 levels using the def2-TZVPPD basis set are also shown with values for other levels in Table 3.

Figure 3. IRMPD spectra from refs. 48 and 49 compared to B3LYP/def2-TZVPPD calculated absorption spectra for conformers of K^+(Lys) (part a) and Cs^+(Lys) (part b) with relative 298 K Gibbs energies calculated at B3LYP/def2, M06/def2, and MP2/def2 levels and, in parentheses, at B3LYP and MP2/6-311++G(2d,2p)//B3LYP/6-31++G(d,p) levels.[49]

Figure 4. Representative zero-pressure extrapolated cross sections for CID of M^+(Lys) (M^+ = Li^+, Na^+, K^+, Rb^+, and Cs^+) with Xe (parts a – e, respectively) as a function of kinetic energy in the center-of-mass frame (lower x-axis) and the laboratory frame (upper x-axis). The experimental data for M^+ are shown by open symbols. Solid lines show the best fit to the experimental data using the model of eq 2, convoluted over the neutral and ion kinetic and internal energy distributions. Dashed lines show the model cross sections in the absence of experimental kinetic energy broadening for reactants with an internal energy of 0 K.

Figure 5. Experimental versus theoretical BDEs (kJ/mol) of M^+(Lys) ($M^+ = Li^+$, Na^+, K^+, Rb^+, and Cs^+). Theoretical values include B3LYP (circles), B3P86 (squares), M06 (open squares), and MP2(full) (triangles). Basis sets used for $M^+ = Li^+$ are aug-cc-pVTZ(Li-C) (blue); for $M^+ = Li^+$, Na^+, and K^+, 6-311+G(2d,2p) (red); and for $M^+ = K^+$, Rb^+, and Cs^+, def2-TZVPPD (green). An alternate experimental value for $M^+ = Li^+$ obtained using the compact lysine conformer is shown by open symbols. The diagonal line shows perfect agreement.

Figure 6. Metal cation-amino acid bond energies for AA = Gly (blue diamonds), Pro (red circles) and Lys (green triangles) versus the inverse of the metal cation radius. Lines are linear regression fits to the data for Cs^+ - Li^+ (excluding Li^+ for Lys) constrained to pass through the origin. The open symbol shows the alternate experimental value for Li^+(Lys) obtained using the compact lysine conformer.

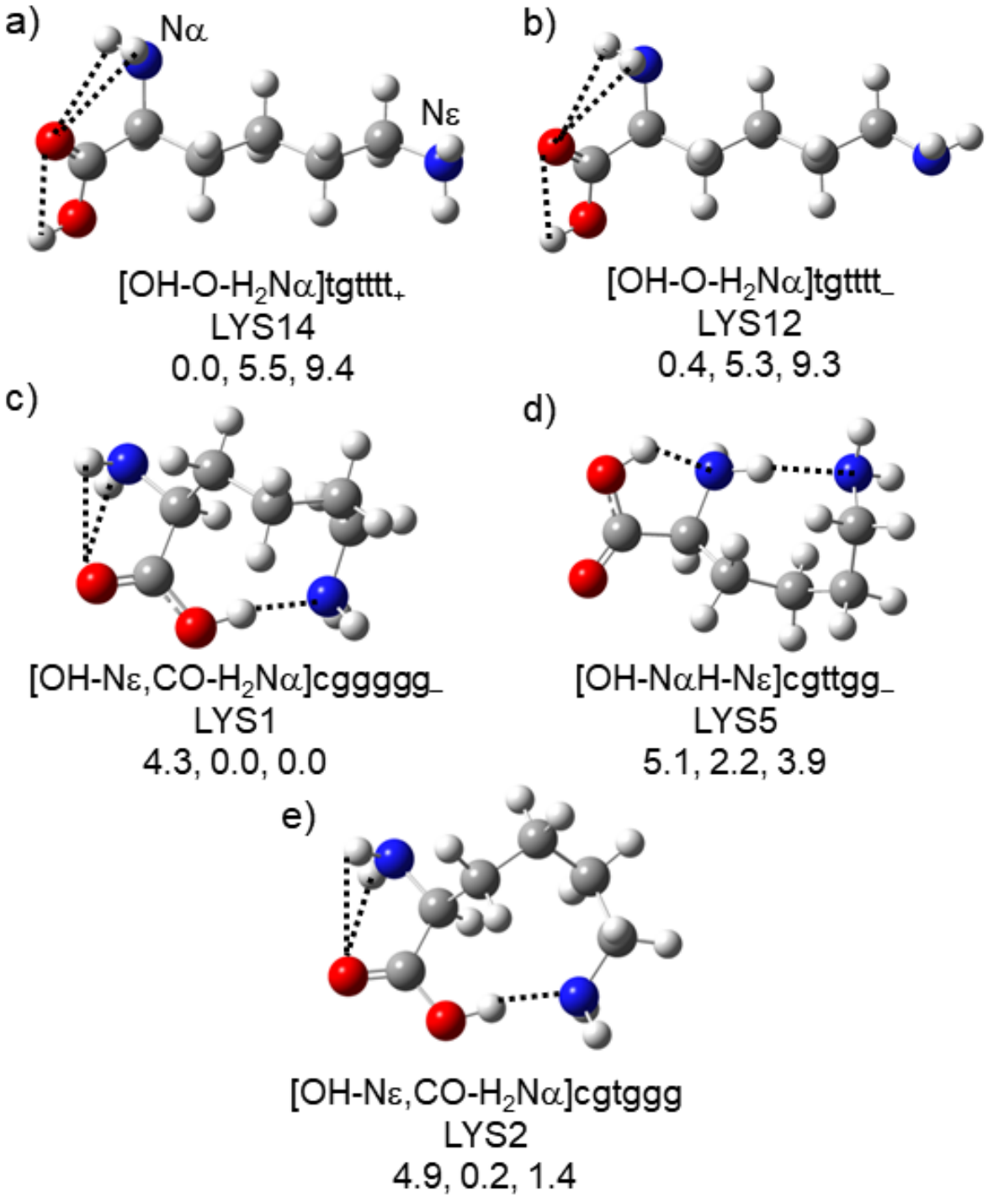
a)
Nα
Nε
[OH-O-H2Nα]tgtttt+
LYS14
0.0, 5.5, 9.4
b)
[OH-O-H2Nα]tgtttt_
LYS12
0.4, 5.3, 9.3
c)
[OH-Nε,CO-H2Nα]cggggg_
LYS1
4.3, 0.0, 0.0
d)
[OH-NαH-Nε]cgttgg_
LYS5
5.1, 2.2, 3.9
e)
[OH-Nε,CO-H2Nα]cgtggg
LYS2
4.9, 0.2, 1.4

Figure 1

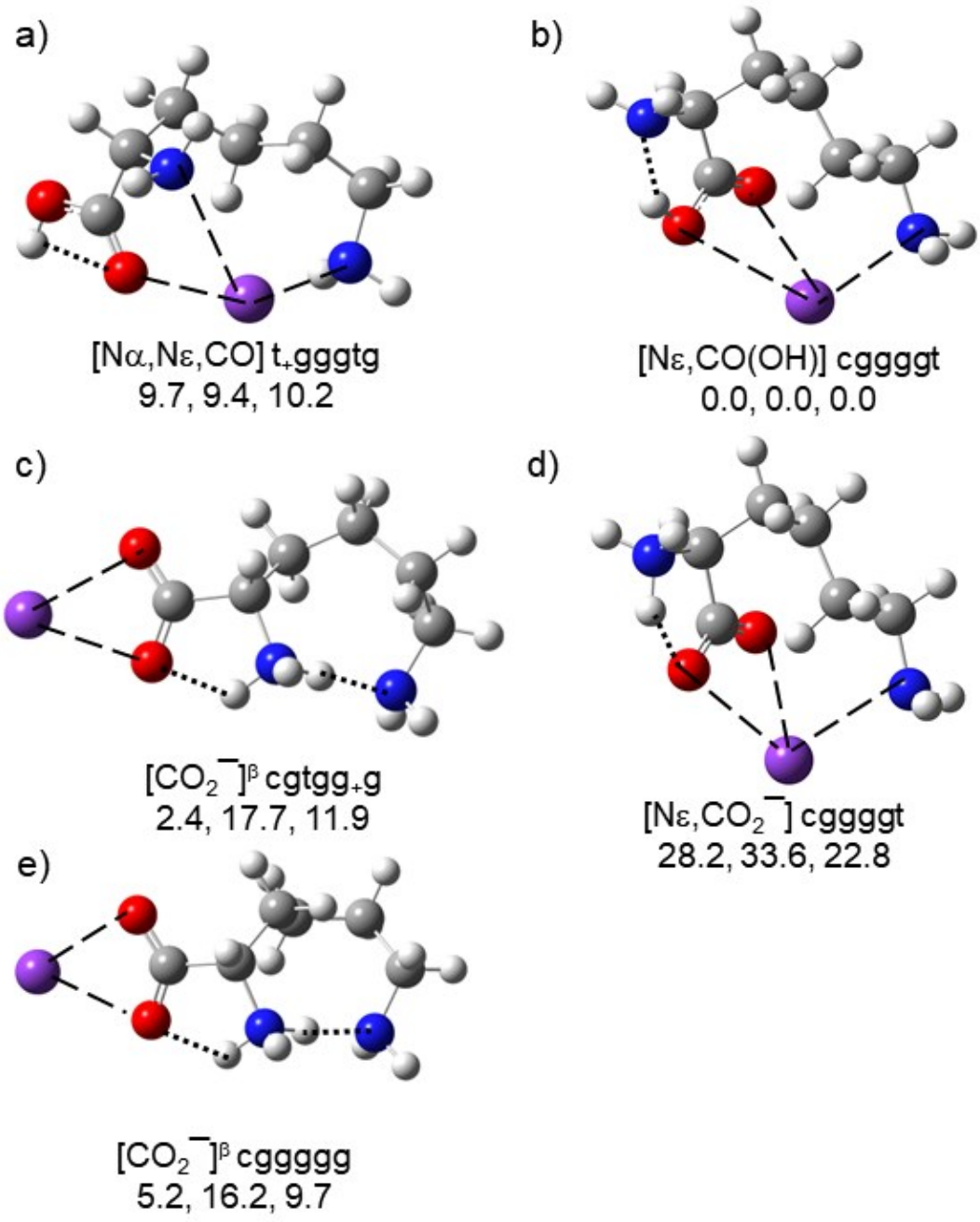
a)
[Nα,Nε,CO] t+gggtg
9.7, 9.4, 10.2
b)
[Nε,CO(OH)] cggggt
0.0, 0.0, 0.0
c)
[CO2¯]β cgtgg+g
2.4, 17.7, 11.9
d)
[Nε,CO2¯] cggggt
28.2, 33.6, 22.8
e)
[CO2¯]β cggggg
5.2, 16.2, 9.7

Figure 2

a)

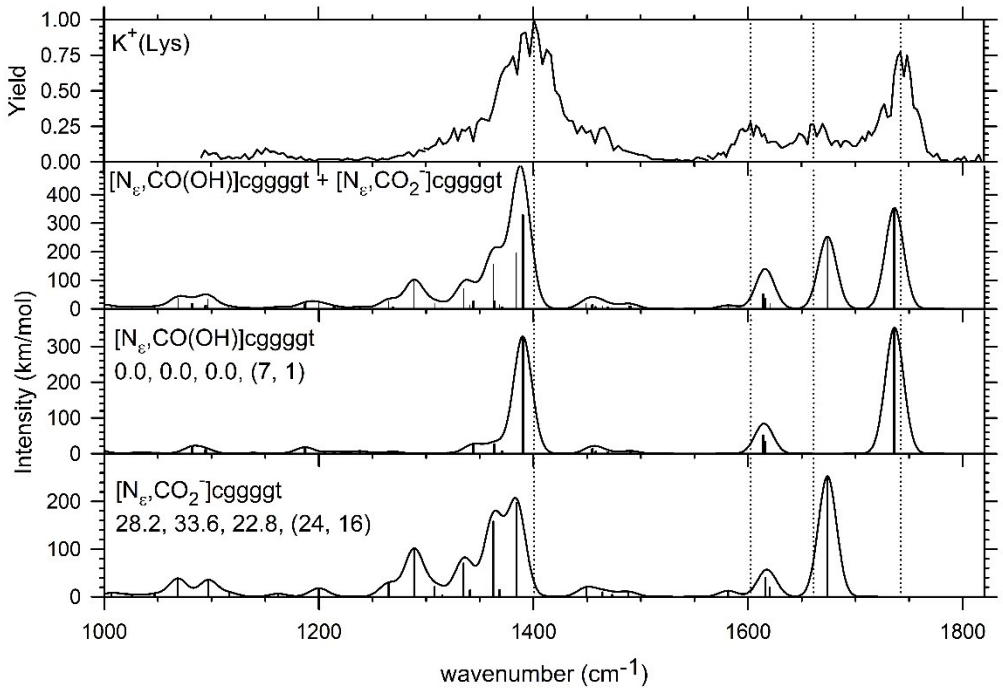
K+(Lys)
Yield
[Nε,CO(OH)]cggggt + [Nε,CO2-]cggggt
[Nε,CO(OH)]cggggt
0.0, 0.0, 0.0, (7, 1)
[Nε,CO2-]cggggt
28.2, 33.6, 22.8, (24, 16)
Intensity (km/mol)
wavenumber (cm-1)

b)

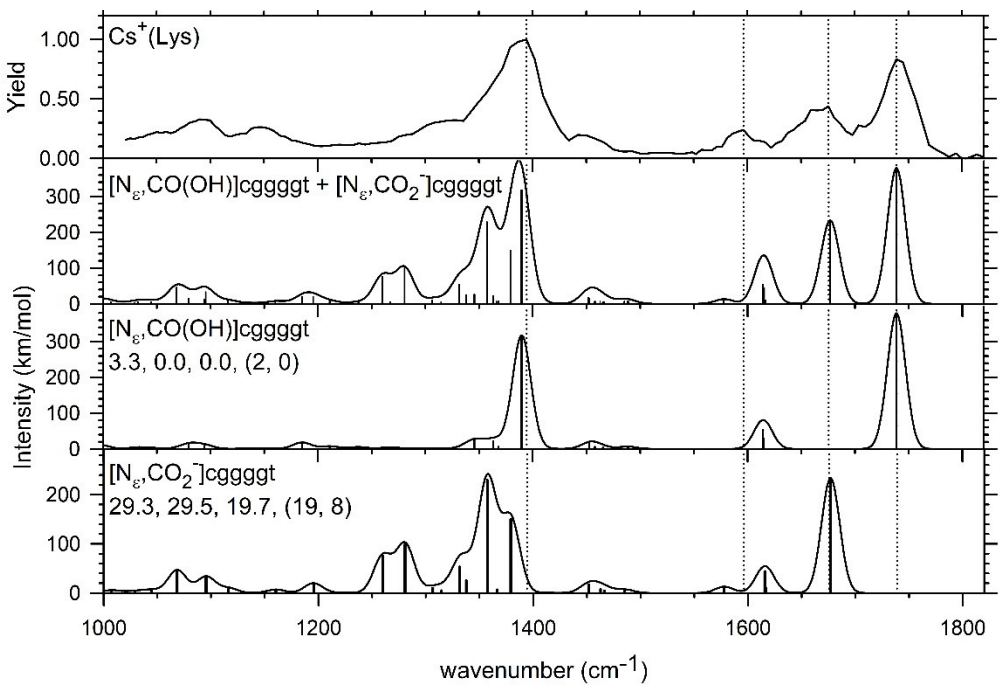
Cs+(Lys)
Yield
[Nε,CO(OH)]cggggt + [Nε,CO2-]cggggt
[Nε,CO(OH)]cggggt
3.3, 0.0, 0.0, (2, 0)
[Nε,CO2-]cggggt
29.3, 29.5, 19.7, (19, 8)
Intensity (km/mol)
wavenumber (cm-1)

Figure 3

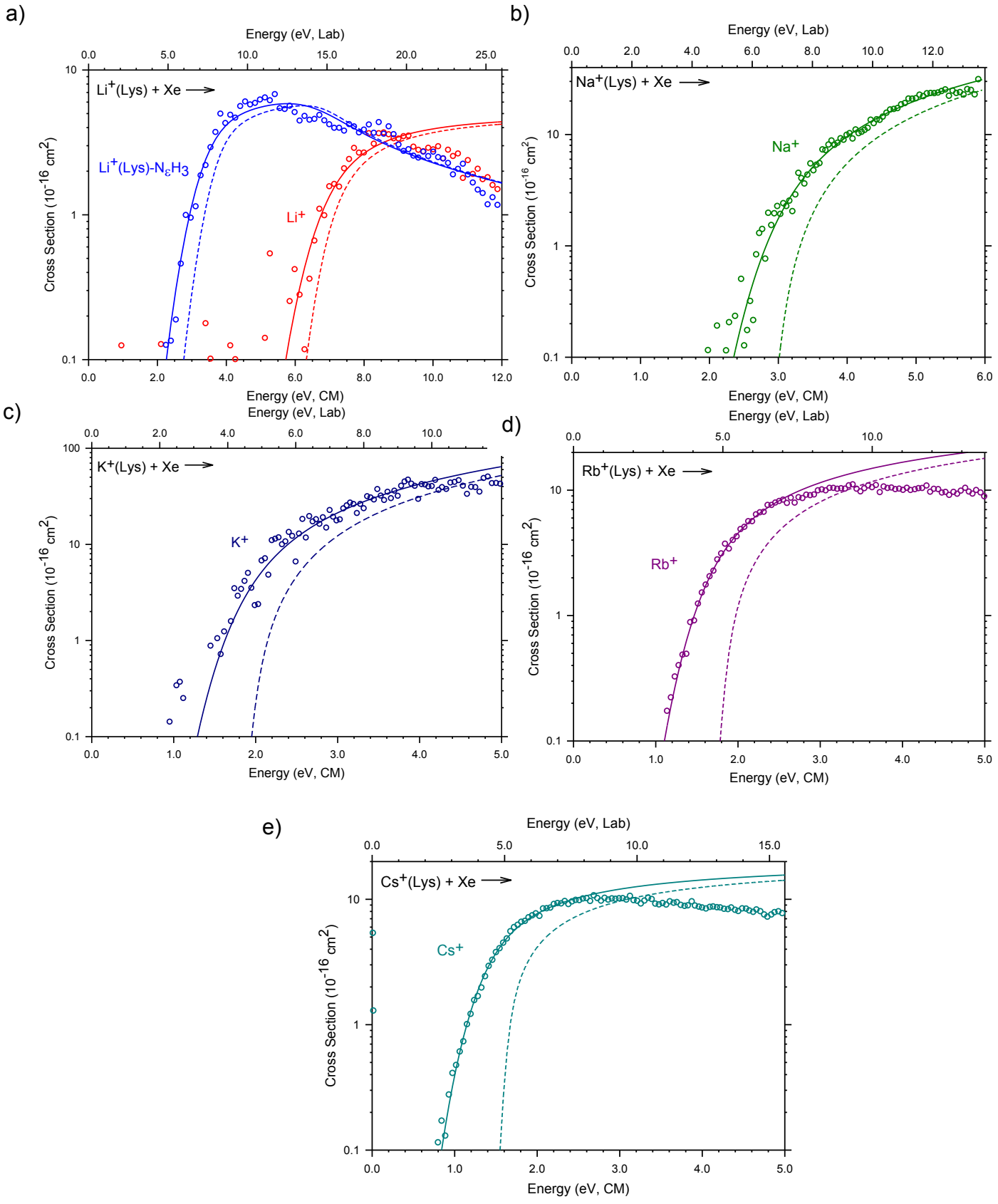
a)
Energy (eV, Lab)
Li+(Lys) + Xe
Li+(Lys)-NεH3
Li+
Cross Section (10-16 cm2)
Energy (eV, CM)
b)
Energy (eV, Lab)
Na+(Lys) + Xe
Na+
Cross Section (10-16 cm2)
Energy (eV, CM)
c)
Energy (eV, Lab)
K+(Lys) + Xe
K+
Cross Section (10-16 cm2)
Energy (eV, CM)
d)
Energy (eV, Lab)
Rb+(Lys) + Xe
Rb+
Cross Section (10-16 cm2)
Energy (eV, CM)
e)
Energy (eV, Lab)
Cs+(Lys) + Xe
Cs+
Cross Section (10-16 cm2)
Energy (eV, CM)

Figure 4

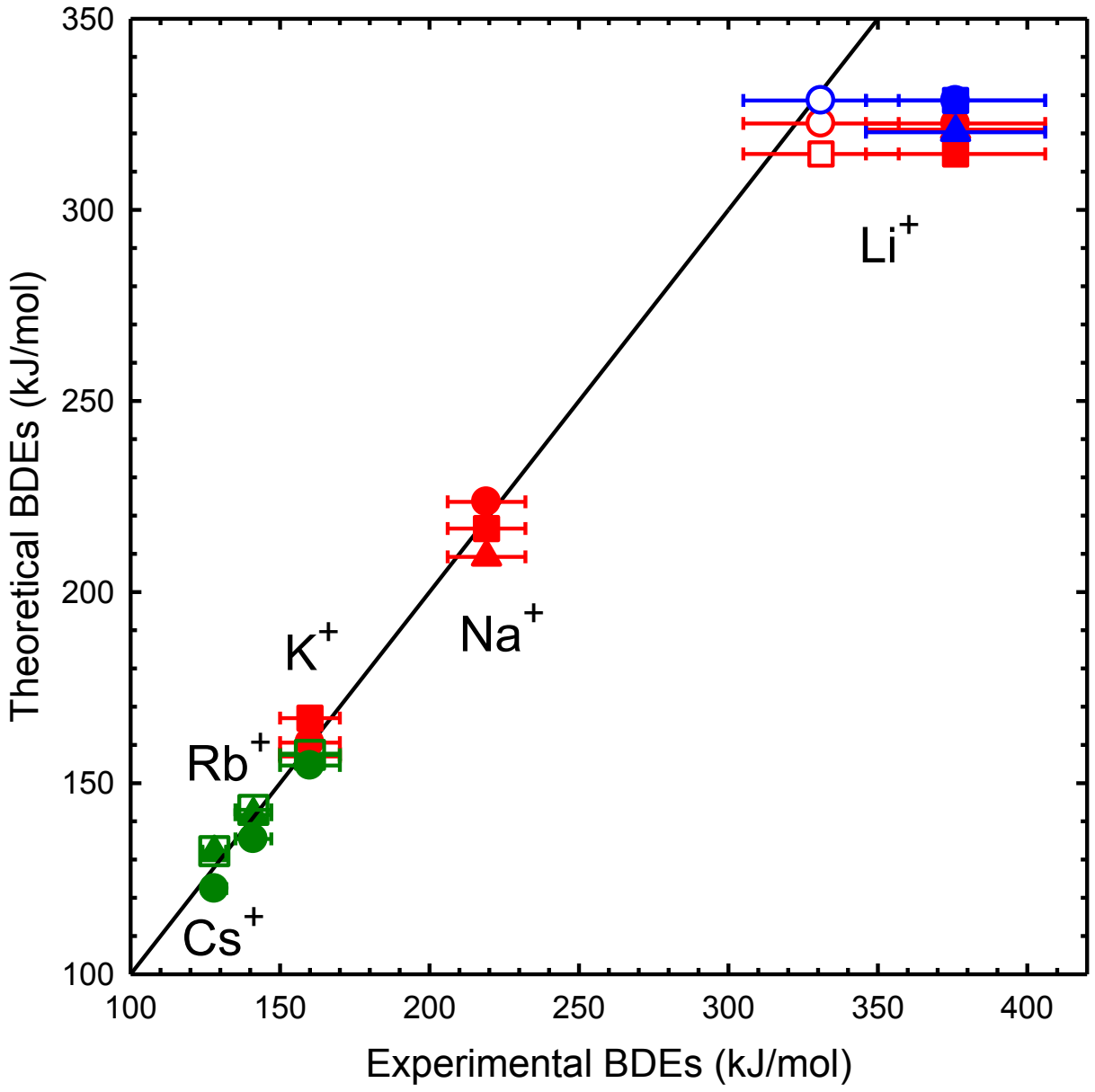
Theoretical BDEs (kJ/mol)
Experimental BDEs (kJ/mol)
100
150
200
250
300
350
400
Li+
Na+
K+
Rb+
Cs+

Figure 5

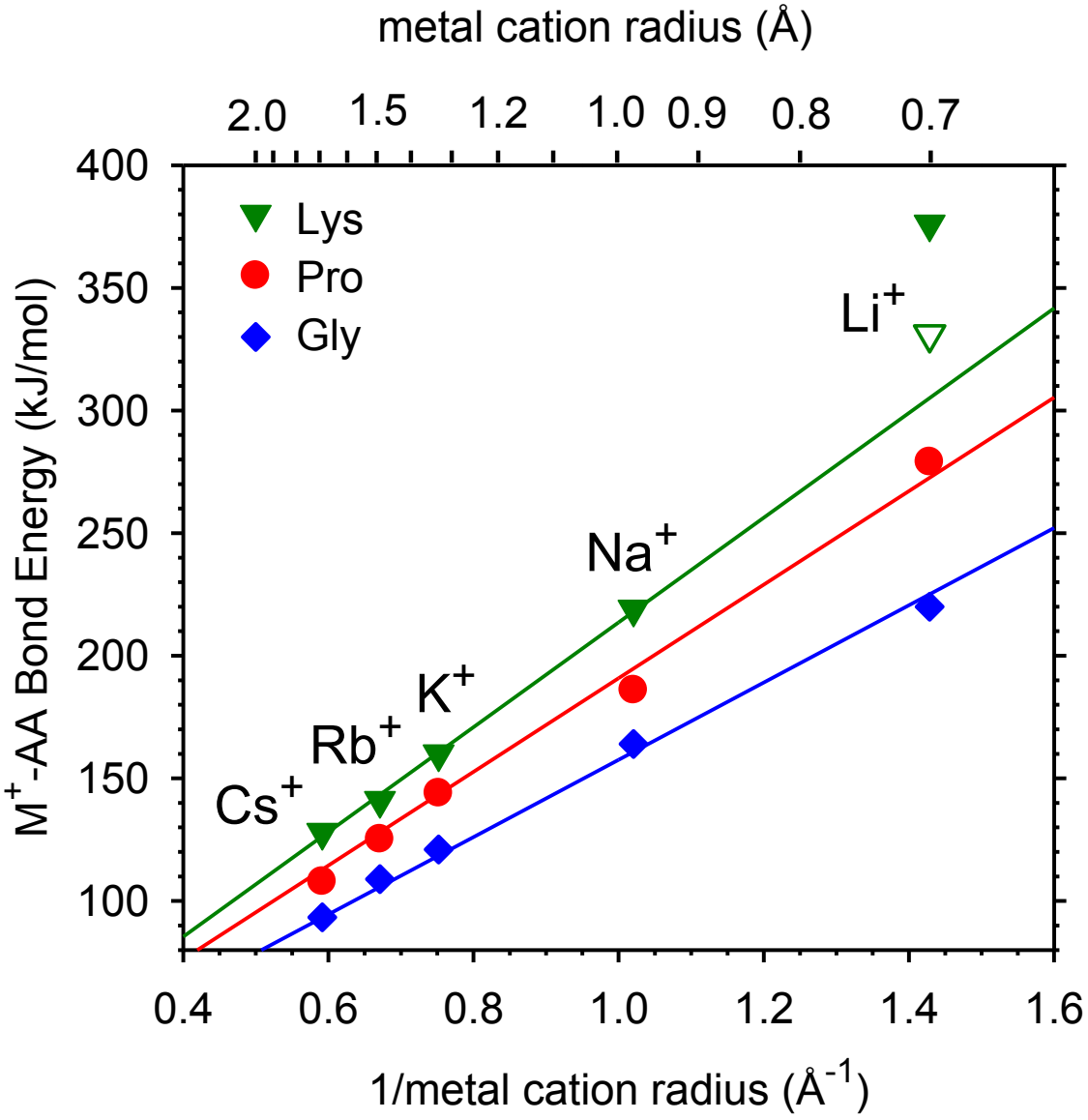
metal cation radius (Å)
2.0
1.5
1.2
1.0
0.9
0.8
0.7
400
350
300
250
200
150
100
M+-AA Bond Energy (kJ/mol)
Lys
Pro
Gly
Li+
Na+
K+
Rb+
Cs+
0.4
0.6
0.8
1.0
1.2
1.4
1.6
1/metal cation radius (Å-1)